Title: Heterosynaptic interactions between dorsal and ventral hippocampus in individual medium spiny neurons of the nucleus accumbens ventromedial shell

Abbreviated title: Interactions between Hipp inputs in the NAc

Authors: Ashley E. Copenhaver[1], Sydnee Vance[1], Sarah A. Snider[1], Kaela Befano[1], J. Branwen She[1], Tara A. LeGates[1,2]

[1] Department of Biological Sciences, University of Maryland, Baltimore County (UMBC)

[2] Department of Pharmacology and Physiology, University of Maryland School of Medicine

Corresponding author:

Tara LeGates, Ph.D.

1000 Hilltop Circle, Interdisciplinary Life Sciences Building 315

Baltimore, MD 21250

tlegates@umbc.edu

Number of pages:

Number of figures: 5 + 2 supplemental figures

Number of words, abstract: 249

Number of words, introduction: 647

Number of words, discussion: 1474

Conflict of interest statement: The authors declare no competing financial interests.

Acknowledgments: We would like to thank Dr. Tagide deCarvalho for her support with microscopy and image analysis, and Dr. Ramesh Chandra for his help with viruses. We would also like to thank Jennifer Pham for her help with injections and Dr. Brian Mathur for his helpful suggestions

on this project. This work was supported by NSF-IOS2402645, T32GM144876-02, T34GM136497, the Merck Academic Fellowship Program, and startup funds provided by UMBC.

ABSTRACT

Establishing learned associations between rewarding stimuli and the context under which those rewards are encountered is critical for survival. Hippocampal input to the nucleus accumbens (NAc) provides important environmental context to reward processing to support goal-directed behaviors. This connection consists of two independent pathways originating from the dorsal (dHipp) or ventral (vHipp) hippocampus, which have previously been considered functionally and anatomically distinct. Here, we show overlap in dHipp and vHipp terminal fields in the NAc, leading us to reconsider this view and raise new questions regarding the potential interactions between dHipp and vHipp pathways in the NAc. Using optogenetics, electrophysiology, and transsynaptic labeling in mice, we investigated anatomical and functional convergence of dHipp and vHipp inputs in the NAc. Transsynaptic labeling revealed a subpopulation of dually innervated cells in the NAc medial shell, confirmed by independent optogenetic manipulation of dHipp and vHipp inputs during whole-cell electrophysiological recordings. Further analysis revealed closely apposed dHipp and vHipp inputs along dendritic branches, and simultaneous stimulation of both inputs elicited heterosynaptic potentiation. Comparison of observed and theoretical success rates suggests interactions between dHipp-NAc and vHipp-NAc synapses may occur presynaptically. Altogether, these results demonstrate that inputs originating from dHipp and vHipp converge onto a subset of NAc neurons with synapses positioned to enable rapid heterosynaptic interactions, indicating integration of these inputs at the single-neuron level. Exploring the physiological and behavioral implications of this convergence will offer new insights into how individual neurons incorporate information from distinct inputs and how this integration may shape learning.

SIGNIFICANCE STATEMENT

Forming associations between rewards and the circumstances under which they are experienced is vital for survival. Hipp input to the NAc is essential for associating rewards with

56 their environmental context to effectively guide motivated behaviors. This connection consists of
57 two separate pathways originating from dHipp and vHipp that have long been considered distinct.
58 Here, we reveal a subpopulation of neurons in the NAc shell innervated by both Hipp subregions
59 as well as heterosynaptic interactions that occur between dHipp and vHipp synapses. These
60 findings suggest that integration of distinct hippocampal information occurs at the single-neuron
61 level, providing a critical mechanism underlying learning and motivated behavior while also
62 opening new avenues for understanding how diverse contextual and reward signals shape
63 decision-making.
64

65 **INTRODUCTION**

66 The integration of diverse information across neural systems is crucial for driving complex
67 behaviors. The brain dynamically integrates information from multiple sources, enabling
68 organisms to react to stimuli and establish learned associations crucial for survival. Plasticity of
69 and interactions between synapses enables coordinated regulation across multiple inputs, critical
70 for orchestrating cell-wide functional responses (Bailey et al., 2000a; Govindarajan et al., 2006a;
71 Harvey & Svoboda, 2007a; Redondo & Morris, 2011a; Schuman & Madison, 1994a). However,
72 the mechanisms underlying how convergent inputs interact to shape neuronal responses remain
73 unclear.

74 The nucleus accumbens (NAc) is a key brain region that integrates diverse information from
75 several brain areas to effectively mediate goal-directed behaviors (Francis & Lobo, 2017; French
76 & Totterdell, 2002; Gruber et al., 2009; Mannella et al., 2013; Marinescu & Labouesse, 2024;
77 Salimpoor et al., 2013; Soares-Cunha et al., 2020). Hippocampal (Hipp) input is a major source
78 of excitatory drive that influences NAc neuron activity (Brog et al., 1993; Calhoon & O'Donnell,
79 2013; Groenewegen et al., 1987; Kelley & Domesick, 1982; Li et al., 2018; O'Donnell & Grace,
80 1995; Phillipson & Griffiths, 1985; Trouche et al., 2019), and because of the Hipp's essential role
81 in contextual and spatial learning (Duarte-Guterman et al., 2015; Lamsa & Lau, 2019; Safari et

82 al., 2021; Savage, 2004; Squire, 1992), Hipp-NAc synapses are also key sites for integrating
83 rewards with related contextual and spatial information. Furthermore, the modulation of the
84 strength of Hipp-NAc synapses is a critical mediator of motivated behaviors and is necessary for
85 supporting contextual- and spatial-based reward learning (Huntley et al., 2020; Ibrahim et al.,
86 2024; Ito et al., 2008, 2008; LeGates et al., 2018; Patterson et al., 2025, p. 202; Pennartz et al.,
87 2011; Sjulson et al., 2018; Trouche et al., 2019; F.-C. Yang & Liang, 2014).

88 The connection between the Hipp and NAc consists of two independent pathways originating
89 from the dorsal and ventral Hipp (dHipp and vHipp), which are considered functionally and
90 anatomically distinct (Amaral & Witter, 1989; Bannerman et al., 2002; Fanselow & Dong, 2010;
91 Friedman et al., 2002; K. B. Kjelstrup et al., 2008; K. G. Kjelstrup et al., 2002; Roberts et al., 2007;
92 Strange et al., 2014). Notably, the NAc is one of the few regions that receives input from both the
93 dHipp and vHipp (Friedman et al., 2002; Kelley & Domesick, 1982; Phillipson & Griffiths, 1985;
94 Trouche et al., 2019). Although dHipp and vHipp are interconnected within the Hipp (Ishizuka et
95 al., 1990; Swanson & Cowan, 1977; Tao et al., 2021), interactions through connections with other
96 brain regions have been proposed as a mechanism linking cognitive and emotional processes
97 (Fanselow & Dong, 2010). In a multifaceted environment, integration of diverse information is
98 important for properly mediating complex behaviors, and the behavioral complexity governed by
99 these pathways warrants synaptic integration to support learning and memory. This is supported
100 by recent findings demonstrating a key role for convergence of dHipp and vHipp input to the
101 amygdala in observational contextual fear memory (Terranova et al., 2022), yet the synaptic basis
102 of this convergence and whether it is also observed in the NAc remains unknown.

103 Using a combination of microscopy, electrophysiology, and optogenetics, we identified and
104 characterized a subpopulation of medium spiny neurons (MSNs) in the medial NAc shell (NAcSh)
105 that are functionally innervated by both the dHipp and vHipp. dHipp and vHipp synapses on dually
106 innervated MSNs have similar basal synaptic properties and are positioned at distances close
107 enough to enable heterosynaptic interactions. These findings suggest that convergent Hipp inputs

108 interact at the synaptic level, which may contribute to the integration of spatial and contextual
109 information to modulate motivated behaviors. Overall, understanding the synaptic integration of
110 dHipp and vHipp inputs in the NAc not only enhances our knowledge of reward-related behaviors,
111 but also offers insight into the fundamental task of neuronal processing and provides a foundation
112 for developing targeted interventions for disorders where these mechanisms are dysregulated.

113 **METHODS**

114 **Animals**

115 Male and female C57BL/6J, Drd1a-tdTomato, Ai14, and Ai195 mice were bred in-house. Mice
116 were housed with same-sex cage mates in a temperature- and humidity-controlled environment
117 under a 12:12 light cycle (lights on at 07:00), with food available *ad libitum*. We did not track
118 estrous cycle in females. All experiments were performed in accordance with the regulations set
119 forth by the Institutional Animal Care and Use Committee at the University of Maryland, Baltimore
120 County.

121

122 **Stereotaxic surgeries**

123 Mice (6-8 weeks old) were anesthetized with 3% isoflurane and underwent stereotaxic
124 surgery. A Hamilton syringe was used to inject adeno-associated viruses (AAV) into the dHipp (in
125 millimeters: from bregma, anterior-posterior (AP), -3.7; medial-lateral (ML), ±2.4; dorsal-ventral
126 (DV), -2.8), vHipp (from bregma, AP, -3.7; ML, ±3.0; DV, -4.8), and NAc (in millimeters: from
127 bregma, anterior-posterior (AP), +1.8; medial-lateral (ML), ±0.6; dorsal-ventral (DV), -4.7). Viruses
128 were injected unilaterally or bilaterally and were infused at a rate of 0.1uL per minute. The injection
129 needle was left in place for 10 minutes following the infusion. After surgery, mice were placed in
130 their home cage on a heating pad for recovery. Carprofen (5mg/kg) was subcutaneously injected
131 daily for 3 days after surgery. Mice recovered for 5-7 weeks for viral expression before anatomical
132 or electrophysiological experiments. Viral constructs pAAV-hSyn-EGFP (Addgene #50465-AAV5)

133 and pAAV-hSyn-mCherry (Addgene #114472-AAV5) were used to visualize dHipp and vHipp
134 axon terminal fields. Anatomical labeling of dually innervated neurons involved the use of
135 pENN.AAV.hSyn.Cre.WPRE.hGH (AAV1, 1013 titer, UMB Viral Vector Core), pAAV-EF1a-Flpo
136 (AAV1, 1013 titer, UMB Viral Vector Core), and pAAV-hSyn-DIO-EGFP (Addgene #50457-AAV2).
137 Specifically, pENN.AAV.hSyn.Cre.WPRE.hGH and pAAV-EF1a-Flpo were injected into the dHipp
138 or vHipp of Ai195 mice for selective labeling of dually innervated neurons.
139 pENN.AAV.hSyn.Cre.WPRE.hGH and pAAV-EF1a-Flpo were injected into the dHipp or vHipp
140 and pAAV-hSyn-DIO-EGFP was injected in the NAc of Ai14 mice to label neurons single and
141 dually innervated neurons. For optogenetic experiments, viral vectors pAAV-Syn-ChrimsonR-tdT
142 (Addgene ID: 59171-AAV5) and either pAAV-Syn-Chronos-GFP (Addgene ID: 59170-AAV5) or
143 pAAV-hSyn-hChR2(H134R)-EYFP (Addgene ID: 26973-AAV5) were used. For all experiments,
144 injection sites were verified by fluorescence microscopy, and brains with off target expression
145 were removed from the experiment.
146
147 **Visualization of axon terminal fields and dually innervated neurons**
148 Mice expressing viruses for anatomical tracing experiments were first anesthetized with
149 isoflurane and then perfused with 1X phosphate buffer solution (PBS), followed by 4%
150 paraformaldehyde (PFA). Brains were removed and post-fixed in 4% PFA overnight at 4ºC and
151 were then transferred to 1X PBS and stored at 4ºC for up to 3 weeks. Brains were sectioned
152 (100µm) using a VT1000S Leica Microsystems vibratome. Slices were then mounted with
153 Vectashield Antifade Mounting Medium on slides for imaging.
154 Images were captured with either a Zeiss LSM 900 Confocal microscope or Zeiss Axio
155 Zoom.V16, both equipped with Zeiss software. To prevent cross talk among channels, images
156 were obtained using sequential scanning to detect multiple fluorophores. To reduce background
157 noise and graininess of images, 2x frame-averaging was used and gain was kept at or below 700.
158 The laser powers used were: EGFP <15% and mCherry or tdTomato <15%. For imaging of

159 dendritic segments, z-stacks with intervals of 0.2μm were acquired and further analyzed using
160 Imaris.

161 To quantify individual and dually innervated neurons, images of dorsomedial NAcSh,
162 ventromedial NAcSh, ventrolateral NAcSh, and ventromedial NAc core were captured on Zeiss
163 LSM 900 Confocal microscope at 40x magnification, equipped with Zeiss software. Images were
164 captured throughout the dorsomedial NAcSh, ventromedial NacSh, ventrolateral NacSh, and
165 ventromedial NAc core. Cells were then manually counted and recounted a day apart. MSNs were
166 identified based on soma size and the presence of highly branched, spiny dendrites, as compared
167 to interneurons, which have larger somas and fewer spines. Analysis and counting were done by
168 an experimenter blinded to conditions.

169 **Acute brain slice preparation for electrophysiology**

170 Acute coronal slices containing the nucleus accumbens or hippocampus were prepared for
171 whole-cell patch-clamp electrophysiology. Hipp-containing slices were kept to verify injection sites
172 before proceeding with electrophysiological experiments in the NAc. Animals were deeply
173 anesthetized with isoflurane, decapitated, and brains were quickly dissected and submerged in
174 ice-cold, bubbled (carbogen: 95% O_2/5% CO_2) *N*-methyl-D-glucamine (NMDG) recovery solution
175 containing the following (in mM): 93 NMDG, 2.5 KCl, 1.2 NaH_2PO_4, 11 glucose, 25 $NaHCO_3$, 1.2
176 $MgCl_2$, and 2.4 $CaCl_2$, pH=7.3-7.4, osmolarity=300-310 mOsm. Using a vibratome (VT1000S,
177 Leica Microsystems), coronal slices (400 μm) were cut in cold, oxygenated NMDG. Slices were
178 transferred to 32-34°C NMDG for 7-12 minutes to recover and were then transferred to room-
179 temperature artificial cerebrospinal fluid (aCSF) containing the following (in mM): 120 NaCl, 3 KCl,
180 1.0 NaH_2PO_4, 20 glucose, 25 $NaHCO_3$, 1.5 $MgCl_2 \cdot 7H_2O$, and 2.5 $CaCl_2$, pH=7.3-7.4. Slices were
181 allowed to recover for 1-hour at room-temperature before beginning electrophysiological
182 recordings.

183 **Whole-cell recordings**

184 We performed whole-cell patch-clamp recordings using an Axopatch 200B amplifier (Axon
185 Instruments, Molecular Devices) and a Digidata 1550B digitizer (Axon Instruments). Slices were
186 placed in a submersion-type recording chamber and superfused with room-temperature aCSF
187 (flow rate 0.5-1mL/min). Patch pipettes (4-8MΩ) were made from borosilicate glass (World
188 Precision Instruments) using a Sutter Instruments P-97 model puller. Cells were visualized using
189 a 60x water immersion objective (Nikon Eclipse FN-1). All recordings were performed in voltage-
190 clamp conditions from MSNs in the NAc ventromedial shell.

191 470nm and 635nm light was used for optogenetic stimulation of Hipp axon terminals in the
192 NAc to record evoked excitatory postsynaptic currents (EPSC). We used light intensities ≤0.5mW
193 to prevent non-specific activation of Chrimson by 470nm light as shown in Figure S1a-b, which
194 aligns with other published studies (Christoffel et al., 2021; Klapoetke et al., 2014; Xia et al.,
195 2020). Similar light intensity ranges were used for 635nm stimulation, and we did not observe
196 non-specific stimulation with this wavelength at any light intensity (Figure S1c-d).

197 For experiments determining I-V relationship and AMPA:NMDA receptor ratios, the patch
198 pipette solution was composed of 135 mM CsCl, 2 mM MgCl6-H2O, 10 mM HEPES, 4 mM Mg-
199 ATP, 0.3 mM Na2-GTP, 10 mM Na2-phosphocreatine, 1 mM EGTA, 5 mM QX-314 bromide, and
200 100 μM spermine; pH=7.3-7.4; osmolarity=285-295mOsm. EPSCs were collected from holding
201 potentials ranging from -80mV to +40mV to create an I-V curve. To calculate AMPA:NMDA
202 receptor ratios, the AMPA component was defined by the peak amplitude at -70mV while the
203 NMDA component was defined by the amplitude at +40mV at 50ms after stimulation. Paired pulse
204 stimulation (100ms ISI) of dHipp or vHipp terminals was alternated every 10s to record EPSCs at
205 dHipp-MSN and vHipp-MSN synapses. PPR was determined by calculating 5-minute averages
206 of EPSC amplitudes from our paired pulses (EPSC1 and EPSC2) and dividing EPSC2 by EPSC1
207 (ie: EPSC2/EPSC1 = PPR). For all other experiments, patch pipettes were filled with a solution

208 containing 130 mM K-gluconate, 5 mM KCl, 2 mM MgCl6-H2O, 10 mM HEPES, 4 mM Mg-ATP,
209 0.3 mM Na2-GTP, 10 mM Na2-phosphocreatine, and 1 mM EGTA; pH=7.3-7.4; osmolarity=285-
210 295mOsm. We used the following exclusion criteria to eliminate unhealthy cells and unreliable
211 recordings: 1) We only proceeded with experiments on cells with series resistances <10MΩ, 2)
212 Cells were excluded if their series resistance changed by >20% (comparing the resistance at the
213 beginning and end of the experiment), 3) Cells in poor health or poor recording status were
214 excluded (i.e. cell partially or fully sealed up, a decrease in holding current >100pA that is
215 consistent with the cell dying, an increase in jitter post HFS, and/or an increase in response failure
216 rate to > 50%).
217
218 **Visualization of dHipp/vHipp terminals with dually innervated neurons**
219 Using a small subset of slices from electrophysiological experiments, dually innervated MSNs
220 were patched and filled with CF633 or CF647 dye (Biotium). Upon completion of electrophysiology
221 experiments, the 400μm-thick slices were fixed in 4% PFA for 4-8 hours at 4ºC. Slices were then
222 mounted in Invitrogen ProLong Glass Antifade Mountant (Thermo Fisher Scientific, #P36980) on
223 slides with spacers (400μm-thick) for imaging. Images were captured with a Zeiss LSM 910
224 confocal microscope equipped with Zeiss software. To prevent cross talk among channels,
225 images were obtained using sequential scanning to detect multiple fluorophores. To reduce
226 background noise and graininess of images, 2x frame-averaging was used and gain was kept at
227 or below 700. The laser powers used were: EGFP <15%, mCherry or tdTomato <15%, CF633
228 <10%. For imaging of dendritic segments and analysis of synapse distributions, z-stacks (0.2μm
229 slices) of distal dendrites were acquired. Surface rendering was conducted using Imaris to create
230 3-dimensional reconstructions of dHipp and vHipp inputs and MSN dendrites. These images were
231 then analyzed in Imaris to identify putative dHipp-MSN and vHipp-MSN synapses and calculate
232 Eucledian distances (edge-to-edge) between nearest neighboring dHipp-MSN and vHipp-MSN
233 synapses along 100μm dendritic segments.

234

235 **Quantification, statistical analysis, and reproducibility**

236 We found no statistically significant difference between males and females, so data from male
237 and females are plotted together. Both the number of cells and number of mice are reported for
238 each experiment. Plots represent the mean ± SEM. The sample size (n) per condition represents
239 the number of cells unless otherwise indicated in the figure caption. Potentiation scores were
240 calculated as the amplitude of the EPSC evoked from synchronous stimulation divided by the sum
241 of the amplitudes from the alternating stimulations. All statistical analyses were performed using
242 Graphpad Prism 9/10 software. Statistical significance ($p<0.05$) was assessed using parametric
243 or non-parametric versions of paired t-tests, or one-way or two-way ANOVA with multiple
244 comparisons. Distributions of nearest neighbor distances were compared to a uniform distribution
245 using a Chi-square goodness of fit test. For box plots, the line in the middle of the box is plotted
246 at the median. The box extends from the 25th to 75th percentiles. Whiskers represent minimum
247 and maximum, and individual data points are shown. Figure schematics and experimental
248 timelines were created with BioRender.com.

249

250 **RESULTS**

251 **dHipp and vHipp axon terminal fields overlap in the NAc medial shell**

252 Using viral-mediated labeling to visualize Hipp neurons and their terminal fields, we examined
253 innervation of the NAc by the posterior dHipp and vHipp. We injected an adenoassociated virus
254 (AAV) expressing eYFP into the dHipp and an AAV expressing mCherry into the vHipp (Figure
255 1a-b). After allowing 5-7 weeks for expression, brains were fixed, sectioned, and imaged using
256 confocal microscopy. We observed dHipp axon terminal fields in the NAc core and lateral shell
257 while the vHipp axon terminal fields were primarily found in the medial shell, in line with previous
258 work (Figure 1c). However, we also observed strong overlap of dHipp and vHipp axon terminal
259 fields in the medial NAcSh (Figure 1c-d), which aligns with the results presented by Brog et al.,

260 1993. 3-D reconstruction of z-stack images of these overlapping axon fields revealed adjacent
261 dHipp and vHipp axons (Figure 1d), highlighting the close proximity of dHipp and vHipp afferents
262 within the medial NAcSh.
263
264 **Identification of NAc neurons dually innervated by the dHipp and vHipp**
265 Given the apposition of dHipp and vHipp terminals, we sought to determine whether individual
266 neurons were innervated by both hippocampal regions. To do this, we utilized transsynaptic
267 expression of Cre and Flp recombinases to selectively target NAc neurons innervated by dHipp
268 and vHipp pathways (Figure 2a). We injected AAV1-hSyn-Cre into the dHipp and AAV1-Ef1a-
269 Flpo into the vHipp of Ai195 mice in which GcaMP6s is only expressed in the presence of Cre
270 and Flp. This approach allowed for targeted expression of GCaMP6s only in neurons that are
271 innervated by both dHipp and vHipp (Figure 2b). After allowing 5-7 weeks for expression, brains
272 were fixed, sectioned and imaged with confocal microscopy using GCaMP6s to visualize dually
273 innervated neurons. Similar to our observations of terminal field overlap, we observed GCaMP6s-
274 expressing cells in the medial NAcSh (Figure 2c), suggesting dual innervation of NAc neurons by
275 both dHipp and vHipp. Furthermore, examination of GCaMP6s-expressing cells revealed
276 morphology similar to MSNs (based on soma size and spiny, highly branched dendrites) (Figure
277 2d), suggesting that individual NAc MSNs receive input from both dHipp and vHipp.
278 To gain better insight into the proportions of cells innervated by dHipp, vHipp, or both, we
279 used our transsynaptic strategy to differentially label cells innervated by dHipp and vHipp.
280 Specifically, we injected AAV1-hSyn-Cre into the dHipp and AAV1-Ef1a-Flpo into the vHipp of
281 Ai14 mice in which there is Cre-dependent expression of tdTomato. We also injected AAV9-Ef1a-
282 fDIO-eYFP into the NAc of these mice (Figure 2e). As a result, cells innervated by dHipp express
283 tdTomato, cells innervated by vHipp express eYFP, and those innervated by both will express
284 both reporters (Figure 2f-g). Quantification of cells in medial NAcSh revealed approximately 8%
285 of cells were innervated by dHipp and vHipp (dually innervated). The remainder of cells were

286 innervated by one Hipp subregion (singly innervated). Of these, 28% cells were innervated by
287 dHipp, 65% were innervated by vHipp (Figure 2h). This suggests that a small proportion of
288 neurons in the medial NAcSh are dually innervated. However, it is worth noting that previous work
289 has reported low efficiency of transsynaptic transport, leading us to believe that our visualization
290 strategy underrepresents the number of dually innervated neurons (Zingg et al., 2017).

291 To independently verify whether individual NAc neurons were dually innervated and determine
292 whether our anatomical results translated into functional convergence, we used optogenetics and
293 whole-cell electrophysiology to independently stimulate dHipp and vHipp inputs while recording
294 from individual NAc neurons. We focused on MSNs because they comprise 95% of the NAc
295 neuron population, align with the morphology of cells identified by our anatomical tracing studies
296 (Figure 2), and have been shown to receive functional input from either dHipp or vHipp in separate
297 studies. To independently stimulate dHipp and vHipp inputs, we used a dual wavelength
298 optogenetic strategy involving viral expression of Chronos and Chrimson, which are maximally
299 sensitive to different wavelengths of light (480nm and 660nm, respectively) (Klapoetke et al.,
300 2014). AAV2-Syn-Chronos-eYFP or AAV2-Syn-Chrimson-mCherry were injected into the dHipp
301 or vHipp. At least 5 weeks after surgery, coronal brain slices containing the NAc were prepared
302 for electrophysiology. Using whole-cell patch-clamp electrophysiology, we recorded from MSNs
303 in the medial NAcSh and used alternating 473 and 635nm light to measure dHipp and vHipp
304 evoked responses in the MSNs. Keeping the light intensity below 1mW prevented cross-
305 contamination, allowing us to measure and independently manipulate dHipp and vHipp inputs
306 with 473 and 635nm light (Figure S1 and 3a). Using this strategy, we identified a subpopulation
307 of MSNs in the medial NAcSh that responded to both dHipp and vHipp stimulation, demonstrating
308 dual functional innervation of individual NAc MSNs by both dHipp and vHipp (Figure 3a). Dually
309 innervated neurons accounted for ~20-50% of neurons surveyed, a greater proportion than that
310 observed with our transsynaptic labeling (Figure 2). The variation in dually innervated neurons

311 appeared to depend on recording site, with higher proportions detected in regions that overlapped
312 with those identified by our labeling approach.

313 Synaptic properties and strengths influence how a neuron responds to and integrates
314 information from distinct inputs, leading us to examine and compare the synaptic profiles of dHipp-
315 MSN and vHipp-MSN synapses in dually innervated neurons. To examine excitatory synaptic
316 strength, we measured AMPAR:NMDAR ratios at dHipp-MSN and vHipp-MSN synapses and
317 found no difference, suggesting that the strength of dHipp- and vHipp-MSN synapses is similar
318 (Figure 3b). We then used paired pulse stimulation, alternating paired pulses such that each
319 pathway was stimulated every 20s, to examine paired-pulse ratios (PPR). PPR was significantly
320 greater at vHipp-MSN synapses as compared to dHipp-MSN synapses (Figure 3c), suggesting
321 potential differences in release probability, though this may be driven by a subpopulation of
322 recorded neurons.

323 Calcium-permeable AMPA receptors (CP-AMPAR) have been identified at ventral subiculum-
324 NAc synapses (Boxer et al., 2023) and have been implicated in NAc plasticity and related
325 behaviors (Carr, 2020; Mameli et al., 2009; McCutcheon et al., 2011; Wolf & Tseng, 2012). Given
326 their role in plasticity and behavior, we examined whether CP-AMPARs were present at dHipp-
327 or vHipp-MSN synapses. Using their characteristic inward rectification and non-linear current-
328 voltage relationship (Cull-Candy et al., 2006; Liu & Zukin, 2007), we performed
329 electrophysiological experiments to identify the predominant population of AMPARs at dHipp and
330 vHipp-MSN synapses. Our results revealed that neither Hipp-MSN synapse contained a
331 significant population of CP-AMPARs (Figure 3d). Collectively, these results indicate that dHipp
332 and vHipp synapses in dually innervated NAc MSNs have comparable basal postsynaptic
333 properties with presynaptic differences in release probability.

334 We then evaluated the potential for synaptic or dendritic-level interactions between dHipp and
335 vHipp synapses by comparing rise times and the spatial locations of putative dHipp and vHipp
336 synapses. Our rise time analysis revealed similar rise times of dHipp- and vHipp-evoked

337 responses, suggesting that dHipp-MSN and vHipp-MSN synapses are located a similar distance
338 away from the cell body (Figure 3e). We filled a subset of cells electrophysiologically confirmed
339 to be dually innervated with a fluorescent dye (Figure 4a), and slices were fixed and prepared for
340 confocal microscopy. We used confocal microscopy and image analysis to measure the spatial
341 location of potential dHipp and vHipp synapses along the dendrites of a dually innervated MSN
342 using the eYFP co-expressed with Chronos, the mCherry co-expressed with Chrimson, and the
343 dye. From this analysis, we found several examples of dHipp and vHipp puncta that are spatially
344 close (<2μm) along distal dendrites of dually innervated MSNs (Figure 4b-c). We analyzed 3-
345 dimensional reconstructions of z-stack images to identify putative dHipp and vHipp inputs on
346 MSNs dendrites and conducted nearest neighbor analysis to measure the spatial relationships
347 between dHipp-MSN and vHipp-MSN synapses. We found that many (>50%) dHipp-MSN and
348 vHipp-MSN synapses are located within a 0-2μm distance (Figure 4d-e), suggesting that dHipp–
349 MSN and vHipp–MSN synapses cluster preferentially near each other. Altogether, these results
350 demonstrate functional innervation of individual MSNs by both dHipp and vHipp, where synapses
351 are frequently observed in close spatial proximity along MSN dendrites.

352 **Heterosynaptic interactions between dHipp and vHipp synapses in NAc MSNs**

353 Synapses that are sufficiently close (<2μm apart) can interact and influence each other's
354 activity (Fu et al., 2012; Harvey & Svoboda, 2007a; Murakoshi et al., 2011; Xia et al., 2020; Yuste,
355 2011). Though activity in dHipp and vHipp is not typically temporally coordinated, learning has
356 been found to increase synchrony between dHipp and vHipp (Biane et al., 2023; Morici et al.,
357 2025). Synchronous activity has been shown to induce plasticity through heterosynaptic
358 interactions between adjacent synapses, raising the question of whether the spatial proximity of
359 dHipp and vHipp synapses facilitates heterosynaptic interactions. To address this, we alternated
360 473nm and 635nm stimulation for 2 minutes to measure EPSCs evoked from independent
361 stimulation of each Hipp pathway. We then synchronized 473nm and 635nm stimulations for 2

362 minutes to record an evoked EPSC from the simultaneous stimulation of both dHipp and vHipp
363 inputs (Figure 5a,b). If no heterosynaptic interactions occur, then the EPSC amplitudes from the
364 alternating stimulation should be the linear sum of the EPSC amplitude evoked by simultaneous
365 stimulation. Instead, our data show a supralinear summation of separately measured EPSCs
366 (Figure 5b), indicating that heterosynaptic potentiation occurs between dHipp and vHipp
367 synapses, an effect observed across multiple light intensities in most cells (Figure S2). We
368 conducted the same experiment in cells that were not dually innervated and found no difference
369 between EPSC amplitudes evoked by alternating and synchronous stimulation, demonstrating
370 that this effect is specific to dually innervated neurons and not a nonspecific artifact resulting from
371 cross-contamination (Figure 5c).

372 To better understand the site of synaptic interaction, we compared the failure rates in a
373 separate experiment using minimal stimulation to evoke pathway-specific responses ~50% of the
374 time so that we could appropriately assess an increase or decrease in failure rate during
375 synchronous stimulation (Figure 5d). We measured EPSCs evoked from alternating and
376 synchronous stimulation of dHipp-MSN and vHipp-MSN synapses. We then calculated the
377 theoretical probability of eliciting a response in both the dHipp- and vHipp-MSN pathways, P_{dual},
378 if they were stimulated at the same time. Assuming the pathways are independent/non-
379 interacting, we can calculate this probability as the product of their individual success properties:
380 $P_{dual}^{theoretical} = P_{dHipp-MSN}^{success} \cdot P_{vHipp-MSN}^{success}$. We compared this theoretical probability to the observed
381 success rate of sync responses that were classified as dual-evoked responses, finding a
382 significant difference in the observed and theoretical values (Figure 5e) suggesting presynaptic
383 mechanisms may facilitate heterosynaptic interactions between dHipp- and vHipp-MSN
384 synapses.

385

386

387 **DISCUSSION**

388 The experiments in this study identified a subpopulation of neurons within the NAc that are
389 dually innervated by dHipp and vHipp. These neurons are primarily located in the NAc
390 ventromedial shell with morphological characteristics that align with those of MSNs. We found
391 that dHipp-MSN and vHipp-MSN synapses in dually innervated neurons have similar basal
392 synaptic properties including comparable release probabilities, synaptic strength, and expression
393 of calcium-impermeable AMPARs. Examination of EPSCs evoked by individual or synchronous
394 stimulation of dHipp and vHipp revealed supralinear summation of EPSCs, suggesting that the
395 synchronous activation of dHipp and vHipp inputs induces short-term heterosynaptic potentiation
396 of dHipp-MSN and vHipp-MSN synapses likely due to presynaptic mechanisms. Altogether, these
397 results reveal mechanisms of dHipp and vHipp synaptic integration within the NAc medial shell,
398 which may be key to supporting the integration of cognitive and emotional processes needed to
399 effectively mediate goal-directed behaviors.

400

401 **Innervation of the NAc by dHipp and vHipp**

402 Our viral-mediated axon terminal field labeling strategy revealed overlapping dHipp and vHipp
403 innervation patterns within the NAc ventromedial shell. At first glance, this finding seems to
404 contradict previous reports that have suggested that the dHipp and vHipp preferentially innervate
405 distinct parts of the NAc. However, these reported innervation patterns appear to depend upon
406 the anterior/posterior coordinate used for Hipp viral injections. Most studies have targeted the
407 posterior vHipp and anterior dHipp, showing vHipp projections in the NAc core and medial shell,
408 with dHipp projections in the NAc core and lateral shell (Groenewegen et al., 1987; Ibrahim et al.,
409 2024; Li et al., 2018; Mulder et al., 1998; Scofield et al., 2016). But when the posterior dHipp was
410 targeted with an anterograde tracer, dHipp axon terminal field expression was observed in the
411 NAc ventromedial shell (Ibrahim et al., 2024). Furthermore, the injection of a retrograde tracer
412 into the NAc ventromedial shell showed that neurons located in the posterior dHipp and vHipp

413 were projecting to this area of the NAc (Groenewegen et al., 1987). Our findings align with the
414 latter two studies, as we injected into the posterior Hipp (A/P: -3.7mm) and found overlapping
415 dHipp and vHipp axon terminal fields and dually innervated neurons primarily in the NAc
416 ventromedial shell.

417 Using a transsynaptic viral-mediated labeling technique, we were able to visualize a small
418 subpopulation of dually innervated neurons that had morphological characteristics similar to
419 MSNs (Figure 2). We confirmed this electrophysiologically, demonstrating that dHipp and vHipp
420 inputs form synaptic connections with individual MSNs within the medial NAcSh (Figure 3).
421 Because this labeling method has low transsynaptic efficiency (Zingg et al., 2017) and requires
422 successful transfer of both Cre and Flp payloads, it likely underrepresents the number of dually
423 innervated neurons. This is supported by our electrophysiology recordings, as within a single
424 slice, we were able to record from a larger number of dually innervated neurons than were
425 indicated from the anatomical tracing study. Further optimization of this transsynaptic approach
426 could improve detection and determine whether sparsely distributed NAc interneurons also
427 receive dual hippocampal input.

428

429 **dHipp and vHipp synapses have similar properties in dually innervated NAc neurons**

430 We found that dHipp- and vHipp-MSN synapses contain primarily calcium-impermeable
431 AMPARs and have similar excitatory synaptic strengths, as measured by AMPA:NMDA receptor
432 ratios (Figure 3). These similarities suggest that, in basal conditions, both pathways may
433 contribute equally to downstream circuit activity. Since the dHipp and vHipp convey different types
434 of behavioral information, this may mean that Hipp-related contextual and sensory cues are
435 equally capable of influencing motivated behaviors. While these similarities are present at
436 baseline, several studies have highlighted changes that occur to dHipp-MSN and vHipp-MSN
437 synapses in response to hormones, neuromodulators, cocaine, external stress, and experience

438 (Floresco et al., 2001; LeGates et al., 2018; Peleg-Raibstein & Feldon, 2006; R. Yang & J.
439 Mogenson, 1984; Sjulson et al., 2018; Williams et al., 2020).
440
441 **Synaptic interactions between distinct Hipp inputs**
442 The NAc is a critical integrator of several major excitatory inputs, many of which exhibit
443 coordinated or synchronous activation (Mahon et al., 2006; Stern et al., 1998). While dHipp and
444 vHipp activity is not typically temporally coordinated, increased synchrony has been associated
445 with learning (Biane et al., 2023; Morici et al., 2025). We found that dHipp-MSN and vHipp-MSN
446 synaptic interactions during simultaneous stimulation elicit heterosynaptic potentiation (Figure 5).
447 Convergent afferent activity and heterosynaptic interactions can alter plasticity thresholds or
448 propagate plastic changes across synapses, fundamentally influencing neuronal information
449 processing and storage (Chistiakova et al., 2015; Reissner et al., 2010). Several mechanisms
450 underlying heterosynaptic plasticity have been identified, including neuromodulator-dependent
451 forms, synaptic tagging and capture, and spatially clustered plasticity, each engaging distinct
452 molecular pathways that ultimately promote plasticity across synapses (Bailey et al., 2000b;
453 Govindarajan et al., 2006b; Harvey & Svoboda, 2007b; Redondo & Morris, 2011b; Schuman &
454 Madison, 1994b). Within the NAc, convergent inputs interact at the synaptic level via a
455 combination of presynaptic and postsynaptic mechanisms to influence behavioral output
456 (O'Donnell & Grace, 1995; Xia et al., 2020; F.-C. Yang & Liang, 2014; Yu et al., 2022). Our
457 analysis of observed and theoretical success rates suggests that dHipp/vHipp heterosynaptic
458 potentiation may occur presynaptically (Figure 5). Axo-axonic synapses in the striatum are rare,
459 but recent work has highlighted heterosynaptic interactions between the basolateral amygdala
460 (BLA), medial prefrontal cortex (mPFC) and paraventricular nucleus of the thalamus (PVT) during
461 co-activation that occur due to presynaptic innervation of mPFC and PVT by BLA (Kornhuber &
462 Kornhuber, 1983; Xia et al., 2020). Additionally, co-activation of vHipp-MSN and BLA-MSN
463 synapses induces long-term potentiation that requires the activity of dopaminergic terminals and

464 D1 receptors (Yu et al., 2022). While this may be due to activity of postsynaptic receptors given
465 that this form of plasticity is more prominent on D1-expressing MSNs, D1 receptors are also
466 expressed presynaptically on glutamatergic terminals and astrocytes where their signaling can
467 alter release probability (Corkrum et al., 2020; Nicola & Malenka, 1997; Zhang et al., 2014).
468

469 **Implications of integration that occurs at the synaptic level**

470 The connection between the Hipp and NAc is crucial for integrating reward with related
471 contextual and spatial information (Britt et al., 2012; Floresco & Phillips, 1999; Humphries &
472 Prescott, 2010; Ito et al., 2008; Lansink et al., 2008, 2009; LeGates et al., 2018; Pennartz et al.,
473 2011; Sjulson et al., 2018). Functional imaging studies in humans have revealed greater Hipp-
474 NAc connectivity associated with positive reinforcement learning (Davidow et al., 2016), increased
475 reward seeking in adolescents (Huntley et al., 2020), and greater positive affect in adults (Heller
476 et al., 2020), implicating a strong link between the strength of Hipp-NAc connectivity and reward-
477 related behaviors. Similar findings have been demonstrated in rodent models which examined
478 Hipp-NAc connectivity using *in vivo* electrophysiology during spatial and contextual-based reward
479 tasks (Sjulson et al., 2018; Sosa et al., 2020; Trouche et al., 2019). The causal relationship
480 between Hipp-NAc connectivity and reward behaviors has been established with lesion and
481 optogenetic studies, demonstrating that Hipp-NAc synapses are required for contextual- and
482 spatial-based reward tasks (Floresco & Phillips, 1999; Ito et al., 2008, p. 200; LeGates et al.,
483 2018; Trouche et al., 2019; Zhou et al., 2019). This includes our previously published work, which
484 demonstrated that the strength of vHipp-NAc synapses is a critical mediator of reward-related
485 behaviors (LeGates et al., 2018).

486 dHipp and vHipp convergence within other areas of the brain has been proposed to be a key
487 circuit mechanism connecting cognitive and emotional processes (Fanselow & Dong, 2010) and
488 may be crucial to establishing and retrieving memories. The dHipp and vHipp are known to convey
489 distinct information critical for driving NAc-mediated motivated behaviors (Ibrahim et al., 2024; Ito

et al., 2008; LeGates et al., 2018; Muir et al., 2020; Patterson et al., 2025; Sjulson et al., 2018; Sosa et al., 2020; Trouche et al., 2019; Williams et al., 2020; A. K. Yang et al., 2020; F.-C. Yang & Liang, 2014). Therefore, the convergence and plasticity we observed may provide a basis by which distinct information conveyed by dHipp and vHipp can shapes the NAc's response to more nuanced contextual and associative information. Similar convergence has been observed in the amygdala, where dHipp and vHipp activate and reactivate, respectively, specific neuron ensembles to mediate contextual fear memory (Terranova et al., 2022). Since Hipp input exerts a strong influence over NAc neuron activity and information flow, it is likely these interactions encourage integration of distinct information conveyed by the dHipp and vHipp, critically impacting behavioral outputs.

Altogether, the results presented here provide evidence for integration of dHipp and vHipp information within individual MSNs of the NAc ventromedial shell. The combination of techniques enabling identification of similar synaptic profiles and rapid interactions occurring between dHipp- and vHipp-MSN synapses provides a foundation for similar studies investigating the integration of distinct inputs at the level of individual neurons. Ultimately, these findings advance our understanding of how spatial and contextual information may contribute to reward-related behaviors while also raising further questions regarding how each of these distinct pathways are regulated.

References

Amaral, D. G., & Witter, M. P. (1989). The three-dimensional organization of the hippocampal formation: A review of anatomical data. *Neuroscience*, *31*(3), 571–591. https://doi.org/10.1016/0306-4522(89)90424-7

Bailey, C. H., Giustetto, M., Huang, Y. Y., Hawkins, R. D., & Kandel, E. R. (2000a). Is heterosynaptic modulation essential for stabilizing Hebbian plasticity and memory? *Nature Reviews. Neuroscience*, *1*(1), 11–20. https://doi.org/10.1038/35036191

Bailey, C. H., Giustetto, M., Huang, Y.-Y., Hawkins, R. D., & Kandel, E. R. (2000b). Is Heterosynaptic modulation essential for stabilizing hebbian plasiticity and memory. *Nature Reviews Neuroscience*, *1*(1), 11–20. https://doi.org/10.1038/35036191

Bannerman, D. M., Deacon, R. M. J., Offen, S., Friswell, J., Grubb, M., & Rawlins, J. N. P. (2002). Double dissociation of function within the hippocampus: Spatial memory and hyponeophagia. *Behavioral Neuroscience*, *116*(5), 884–901. https://doi.org/10.1037/0735-7044.116.5.884

Biane, J. S., Ladow, M. A., Stefanini, F., Boddu, S. P., Fan, A., Hassan, S., Dundar, N., Apodaca-Montano, D. L., Zhou, L. Z., Fayner, V., Woods, N. I., & Kheirbek, M. A. (2023). Neural dynamics underlying associative learning in the dorsal and ventral hippocampus. *Nature Neuroscience*, *26*(5), 798–809. https://doi.org/10.1038/s41593-023-01296-6

Boxer, E. E., Kim, J., Dunn, B., & Aoto, J. (2023). Ventral Subiculum Inputs to Nucleus Accumbens Medial Shell Preferentially Innervate D2R Medium Spiny Neurons and Contain Calcium Permeable AMPARs. *The Journal of Neuroscience*, *43*(7), 1166–1177. https://doi.org/10.1523/JNEUROSCI.1907-22.2022

Britt, J. P., Benaliouad, F., McDevitt, R. A., Stuber, G. D., Wise, R. A., & Bonci, A. (2012). Synaptic and Behavioral Profile of Multiple Glutamatergic Inputs to the Nucleus Accumbens. *Neuron*, *76*(4), 790–803. https://doi.org/10.1016/j.neuron.2012.09.040

Brog, J. S., Salyapongse, A., Deutch, A. Y., & Zahm, D. S. (1993). The patterns of afferent innervation of the core and shell in the “Accumbens” part of the rat ventral striatum: Immunohistochemical detection of retrogradely transported fluoro-gold. *Journal of Comparative Neurology*, *338*(2), 255–278. https://doi.org/10.1002/cne.903380209

Calhoon, G. G., & O’Donnell, P. (2013). Closing the Gate in the Limbic Striatum: Prefrontal Suppression of Hippocampal and Thalamic Inputs. *Neuron*, *78*(1), 181–190. https://doi.org/10.1016/j.neuron.2013.01.032

Carr, K. D. (2020). Homeostatic regulation of reward via synaptic insertion of calcium-permeable AMPA receptors in nucleus accumbens. *Physiology & Behavior*, *219*, 112850. https://doi.org/10.1016/j.physbeh.2020.112850

Chistiakova, M., Bannon, N., Chen, J.-Y., Bazhenov, M., & Volgushev, M. (2015). Homeostatic role of heterosynaptic plasticity: Models and experiments. *Frontiers in Computational Neuroscience*, *9*. https://www.frontiersin.org/articles/10.3389/fncom.2015.00089

Christoffel, D. J., Walsh, J. J., Hoerbelt, P., Heifets, B. D., Llorach, P., Lopez, R. C., Ramakrishnan, C., Deisseroth, K., & Malenka, R. C. (2021). Selective filtering of excitatory inputs to nucleus accumbens by dopamine and serotonin. *Proceedings of the National Academy of Sciences*, *118*(24), e2106648118. https://doi.org/10.1073/pnas.2106648118

Corkrum, M., Covelo, A., Lines, J., Bellocchio, L., Pisansky, M., Loke, K., Quintana, R., Rothwell, P. E., Lujan, R., Marsicano, G., Martin, E. D., Thomas, M. J., Kofuji, P., & Araque, A. (2020). Dopamine-Evoked Synaptic Regulation in the Nucleus Accumbens Requires Astrocyte Activity. *Neuron*, *105*(6), 1036-1047.e5. https://doi.org/10.1016/j.neuron.2019.12.026

Cull-Candy, S., Kelly, L., & Farrant, M. (2006). Regulation of Ca2+-permeable AMPA receptors: Synaptic plasticity and beyond. *Current Opinion in Neurobiology*, *16*(3), 288–297. https://doi.org/10.1016/j.conb.2006.05.012

Davidow, J. Y., Foerde, K., Galván, A., & Shohamy, D. (2016). An Upside to Reward Sensitivity: The Hippocampus Supports Enhanced Reinforcement Learning in Adolescence. *Neuron*, *92*(1), 93–99. https://doi.org/10.1016/j.neuron.2016.08.031

Duarte-Guterman, P., Yagi, S., Chow, C., & Galea, L. A. M. (2015). Hippocampal learning, memory, and neurogenesis: Effects of sex and estrogens across the lifespan in adults. *Hormones and Behavior*, *74*, 37–52. https://doi.org/10.1016/j.yhbeh.2015.05.024

Fanselow, M. S., & Dong, H.-W. (2010). Are The Dorsal and Ventral Hippocampus functionally distinct structures? *Neuron*, *65*(1), 7. https://doi.org/10.1016/j.neuron.2009.11.031

Floresco, S. B., Blaha, C. D., Yang, C. R., & Phillips, A. G. (2001). Modulation of Hippocampal and Amygdalar-Evoked Activity of Nucleus Accumbens Neurons by Dopamine: Cellular Mechanisms of Input Selection. *The Journal of Neuroscience*, *21*(8), 2851–2860. https://doi.org/10.1523/JNEUROSCI.21-08-02851.2001

Floresco, S. B., & Phillips, A. G. (1999). Dopamine and hippocampal input to the nucleus accumbens play an essential role in the search for food in an unpredictable environment. *Psychobiology*, *27*(2), 277–286. https://doi.org/10.3758/BF03332121

Francis, T. C., & Lobo, M. K. (2017). Emerging Role for Nucleus Accumbens Medium Spiny Neuron Subtypes in Depression. *Biological Psychiatry*, *81*(8), 645–653. https://doi.org/10.1016/j.biopsych.2016.09.007

French, S. J., & Totterdell, S. (2002). Hippocampal and prefrontal cortical inputs monosynaptically converge with individual projection neurons of the nucleus accumbens. *The Journal of Comparative Neurology*, *446*(2), 151–165. https://doi.org/10.1002/cne.10191

Friedman, D. P., Aggleton, J. P., & Saunders, R. C. (2002). Comparison of hippocampal, amygdala, and perirhinal projections to the nucleus accumbens: Combined anterograde and retrograde tracing study in the Macaque brain. *Journal of Comparative Neurology*, *450*(4), 345–365. https://doi.org/10.1002/cne.10336

Fu, M., Yu, X., Lu, J., & Zuo, Y. (2012). Repetitive motor learning induces coordinated formation of clustered dendritic spines in vivo. *Nature*, *483*(7387), 92–95. https://doi.org/10.1038/nature10844

Govindarajan, A., Kelleher, R. J., & Tonegawa, S. (2006a). A clustered plasticity model of long-term memory engrams. *Nature Reviews. Neuroscience*, *7*(7), 575–583. https://doi.org/10.1038/nrn1937

Govindarajan, A., Kelleher, R. J., & Tonegawa, S. (2006b). A clustered plasticity model of long-term memory engrams. *Nature Reviews Neuroscience*, *7*(7), 575–583. https://doi.org/10.1038/nrn1937

Groenewegen, H. J., Der Zee, E. V.-V., Te Kortschot, A., & Witter, M. P. (1987). Organization of the projections from the subiculum to the ventral striatum in the rat. A study using anterograde transport of Phaseolus vulgaris leucoagglutinin. *Neuroscience*, *23*(1), 103–120. https://doi.org/10.1016/0306-4522(87)90275-2

Gruber, A. J., Hussain, R. J., & O'Donnell, P. (2009). The Nucleus Accumbens: A Switchboard for Goal-Directed Behaviors. *PLoS ONE*, *4*(4), e5062. https://doi.org/10.1371/journal.pone.0005062

Harvey, C. D., & Svoboda, K. (2007a). Locally dynamic synaptic learning rules in pyramidal neuron dendrites. *Nature*, *450*(7173), 1195–1200. https://doi.org/10.1038/nature06416

Harvey, C. D., & Svoboda, K. (2007b). Locally dynamic synaptic learning rules in pyramidal neuron dendrites. *Nature*, *450*(7173), 1195–1200. https://doi.org/10.1038/nature06416

Heller, A. S., Shi, T. C., Ezie, C. E. C., Reneau, T. R., Baez, L. M., Gibbons, C. J., & Hartley, C. A. (2020). Association between real-world experiential diversity and positive affect relates to hippocampal–striatal functional connectivity. *Nature Neuroscience*, *23*(7), 800–804. https://doi.org/10.1038/s41593-020-0636-4

Humphries, M. D., & Prescott, T. J. (2010). The ventral basal ganglia, a selection mechanism at the crossroads of space, strategy, and reward. *Progress in Neurobiology*, *90*(4), 385–417. https://doi.org/10.1016/j.pneurobio.2009.11.003

Huntley, E. D., Marusak, H. A., Berman, S. E., Zundel, C. G., Hatfield, J. R. B., Keating, D. P., & Rabinak, C. A. (2020). Adolescent substance use and functional connectivity between the ventral striatum and hippocampus. *Behavioural Brain Research*, *390*, 112678. https://doi.org/10.1016/j.bbr.2020.112678

Ibrahim, K. M., Massaly, N., Yoon, H.-J., Sandoval, R., Widman, A. J., Heuermann, R. J., Williams, S., Post, W., Pathiranage, S., Lintz, T., Zec, A., Park, A., Yu, W., Kash, T. L., Gereau, R. W., & Morón, J. A. (2024). Dorsal hippocampus to nucleus accumbens projections drive reinforcement via activation of accumbal dynorphin neurons. *Nature Communications*, *15*(1), 750. https://doi.org/10.1038/s41467-024-44836-9

Ishizuka, N., Weber, J., & Amaral, D. G. (1990). Organization of intrahippocampal projections originating from CA3 pyramidal cells in the rat. *Journal of Comparative Neurology*, *295*(4), 580–623. https://doi.org/10.1002/cne.902950407

Ito, R., Robbins, T. W., Pennartz, C. M., & Everitt, B. J. (2008). Functional Interaction between the Hippocampus and Nucleus Accumbens Shell Is Necessary for the Acquisition of Appetitive Spatial Context Conditioning. *Journal of Neuroscience*, *28*(27), 6950–6959. https://doi.org/10.1523/JNEUROSCI.1615-08.2008

Kelley, A. E., & Domesick, V. B. (1982). The distribution of the projection from the hippocampal formation to the nucleus accumbens in the rat: An anterograde and retrograde-horseradish peroxidase study. *Neuroscience*, *7*(10), 2321–2335. https://doi.org/10.1016/0306-4522(82)90198-1

Kjelstrup, K. B., Solstad, T., Brun, V. H., Hafting, T., Leutgeb, S., Witter, M. P., Moser, E. I., & Moser, M.-B. (2008). Finite Scale of Spatial Representation in the Hippocampus. *Science*, *321*(5885), 140–143. https://doi.org/10.1126/science.1157086

Kjelstrup, K. G., Tuvnes, F. A., Steffenach, H.-A., Murison, R., Moser, E. I., & Moser, M.-B. (2002). Reduced fear expression after lesions of the ventral hippocampus. *Proceedings of the National Academy of Sciences*, *99*(16), 10825–10830. https://doi.org/10.1073/pnas.152112399

Klapoetke, N. C., Murata, Y., Kim, S. S., Pulver, S. R., Birdsey-Benson, A., Cho, Y. K., Morimoto, T. K., Chuong, A. S., Carpenter, E. J., Tian, Z., Wang, J., Xie, Y., Yan, Z., Zhang, Y., Chow, B. Y., Surek, B., Melkonian, M., Jayaraman, V., Constantine-Paton, M., … Boyden, E. S. (2014). Independent optical excitation of distinct neural populations. *Nature Methods*, *11*(3), 338–346. https://doi.org/10.1038/nmeth.2836

Kornhuber, J., & Kornhuber, M. E. (1983). Axo-axonic synapses in the rat striatum. *European Neurology*, *22*(6), 433–436. https://doi.org/10.1159/000115598

Lamsa, K., & Lau, P. (2019). Long-term plasticity of hippocampal interneurons during in vivo memory processes. *Current Opinion in Neurobiology*, *54*, 20–27. https://doi.org/10.1016/j.conb.2018.08.006

Lansink, C. S., Goltstein, P. M., Lankelma, J. V., Joosten, R. N. J. M. A., McNaughton, B. L., & Pennartz, C. M. A. (2008). Preferential Reactivation of Motivationally Relevant Information in the Ventral Striatum. *Journal of Neuroscience*, *28*(25), 6372–6382. https://doi.org/10.1523/JNEUROSCI.1054-08.2008

Lansink, C. S., Goltstein, P. M., Lankelma, J. V., McNaughton, B. L., & Pennartz, C. M. A. (2009). Hippocampus Leads Ventral Striatum in Replay of Place-Reward Information. *PLoS Biology*, *7*(8), e1000173. https://doi.org/10.1371/journal.pbio.1000173

LeGates, T. A., Kvarta, M. D., Tooley, J. R., Francis, T. C., Lobo, M. K., Creed, M. C., & Thompson, S. M. (2018). Reward behaviour is regulated by the strength of hippocampus–nucleus accumbens synapses. *Nature*, *564*(7735), 258–262. https://doi.org/10.1038/s41586-018-0740-8

660 Li, Z., Chen, Z., Fan, G., Li, A., Yuan, J., & Xu, T. (2018). Cell-Type-Specific Afferent
661 Innervation of the Nucleus Accumbens Core and Shell. *Frontiers in Neuroanatomy*, *12*,
662 84. https://doi.org/10.3389/fnana.2018.00084
663 Liu, S. J., & Zukin, R. S. (2007). Ca2+-permeable AMPA receptors in synaptic plasticity and
664 neuronal death. *Trends in Neurosciences*, *30*(3), 126–134.
665 https://doi.org/10.1016/j.tins.2007.01.006
666 Mahon, S., Vautrelle, N., Pezard, L., Slaght, S. J., Deniau, J.-M., Chouvet, G., & Charpier, S.
667 (2006). Distinct Patterns of Striatal Medium Spiny Neuron Activity during the Natural
668 Sleep–Wake Cycle. *Journal of Neuroscience*, *26*(48), 12587–12595.
669 https://doi.org/10.1523/JNEUROSCI.3987-06.2006
670 Mameli, M., Halbout, B., Creton, C., Engblom, D., Parkitna, J. R., Spanagel, R., & Lüscher, C.
671 (2009). Cocaine-evoked synaptic plasticity: Persistence in the VTA triggers adaptations
672 in the NAc. *Nature Neuroscience*, *12*(8), 1036–1041. https://doi.org/10.1038/nn.2367
673 Mannella, F., Gurney, K., & Baldassarre, G. (2013). The nucleus accumbens as a nexus
674 between values and goals in goal-directed behavior: A review and a new hypothesis.
675 *Frontiers in Behavioral Neuroscience*, *7*. https://doi.org/10.3389/fnbeh.2013.00135
676 Marinescu, A.-M., & Labouesse, M. A. (2024). The nucleus accumbens shell: A neural hub at
677 the interface of homeostatic and hedonic feeding. *Frontiers in Neuroscience*, *18*,
678 1437210. https://doi.org/10.3389/fnins.2024.1437210
679 McCutcheon, J. E., Wang, X., Tseng, K. Y., Wolf, M. E., & Marinelli, M. (2011). Calcium-
680 Permeable AMPA Receptors Are Present in Nucleus Accumbens Synapses after
681 Prolonged Withdrawal from Cocaine Self-Administration But Not Experimenter-
682 Administered Cocaine. *The Journal of Neuroscience*, *31*(15), 5737–5743.
683 https://doi.org/10.1523/JNEUROSCI.0350-11.2011

Morici, J. F., Paiva-Lima, I., Silva, A., Pronier, É., & Girardeau, G. (2025). *Dorso-ventral hippocampus neural assemblies reactivate during sleep following an aversive experience* (p. 2024.06.13.598918). bioRxiv. https://doi.org/10.1101/2024.06.13.598918

Muir, J., Tse, Y. C., Iyer, E. S., Biris, J., Cvetkovska, V., Lopez, J., & Bagot, R. C. (2020). Ventral Hippocampal Afferents to Nucleus Accumbens Encode Both Latent Vulnerability and Stress-Induced Susceptibility. *Biological Psychiatry*, *88*(11), 843–854. https://doi.org/10.1016/j.biopsych.2020.05.021

Mulder, A. B., Hodenpijl, M. G., & Lopes Da Silva, F. H. (1998). Electrophysiology of the Hippocampal and Amygdaloid Projections to the Nucleus Accumbens of the Rat: Convergence, Segregation, and Interaction of Inputs. *The Journal of Neuroscience*, *18*(13), 5095–5102. https://doi.org/10.1523/JNEUROSCI.18-13-05095.1998

Murakoshi, H., Wang, H., & Yasuda, R. (2011). Local, persistent activation of Rho GTPases during plasticity of single dendritic spines. *Nature*, *472*(7341), 100–104. https://doi.org/10.1038/nature09823

Nicola, S. M., & Malenka, R. C. (1997). Dopamine Depresses Excitatory and Inhibitory Synaptic Transmission by Distinct Mechanisms in the Nucleus Accumbens. *Journal of Neuroscience*, *17*(15), 5697–5710. https://doi.org/10.1523/JNEUROSCI.17-15-05697.1997

O'Donnell, P., & Grace, A. (1995). Synaptic interactions among excitatory afferents to nucleus accumbens neurons: Hippocampal gating of prefrontal cortical input. *The Journal of Neuroscience*, *15*(5), 3622–3639. https://doi.org/10.1523/JNEUROSCI.15-05-03622.1995

Patterson, D., Khan, N., Collins, E. A., Stewart, N. R., Sassaninejad, K., Yeates, D., Lee, A. C. H., & Ito, R. (2025). Ventral hippocampus to nucleus accumbens shell circuit regulates approach decisions during motivational conflict. *PLOS Biology*, *23*(1), e3002722. https://doi.org/10.1371/journal.pbio.3002722

Paxinos, G., & Franklin, K. B. J. (2019). *Paxinos and Franklin's The mouse brain in stereotaxic coordinates* (Fifth edition). Academic Press, an imprint of Elsevier.

Peleg-Raibstein, D., & Feldon, J. (2006). Effects of dorsal and ventral hippocampal NMDA stimulation on nucleus accumbens core and shell dopamine release. *Neuropharmacology*, *51*(5), 947–957. https://doi.org/10.1016/j.neuropharm.2006.06.002

Pennartz, C. M. A., Ito, R., Verschure, P. F. M. J., Battaglia, F. P., & Robbins, T. W. (2011). The hippocampal–striatal axis in learning, prediction and goal-directed behavior. *Trends in Neurosciences*, *34*(10), 548–559. https://doi.org/10.1016/j.tins.2011.08.001

Phillipson, O. T., & Griffiths, A. C. (1985). The topographic order of inputs to nucleus accumbens in the rat. *Neuroscience*, *16*(2), 275–296. https://doi.org/10.1016/0306-4522(85)90002-8

R. Yang, C., & J. Mogenson, G. (1984). Electrophysiological responses of neurones in the nucleus accumbens to hippocampal stimulation and the attenuation of the excitatory responses by the mesolimbic dopaminergic system. *Brain Research*, *324*(1), 69–84. https://doi.org/10.1016/0006-8993(84)90623-1

Redondo, R. L., & Morris, R. G. M. (2011a). Making memories last: The synaptic tagging and capture hypothesis. *Nature Reviews. Neuroscience*, *12*(1), 17–30. https://doi.org/10.1038/nrn2963

Redondo, R. L., & Morris, R. G. M. (2011b). Making memories last: The synaptic tagging and capture hypothesis. *Nature Reviews Neuroscience*, *12*(1), 17–30. https://doi.org/10.1038/nrn2963

Reissner, K. J., Pu, L., Schaffhausen, J. H., Boyle, H. D., Smith, I. F., Parker, I., & Carew, T. J. (2010). A Novel Postsynaptic Mechanism for Heterosynaptic Sharing of Short-Term Plasticity. *Journal of Neuroscience*, *30*(26), 8797–8806. https://doi.org/10.1523/JNEUROSCI.4767-09.2010

Roberts, A. C., Tomic, D. L., Parkinson, C. H., Roeling, T. A., Cutter, D. J., Robbins, T. W., & Everitt, B. J. (2007). Forebrain connectivity of the prefrontal cortex in the marmoset monkey (*Callithrix jacchus*): An anterograde and retrograde tract-tracing study. *Journal of Comparative Neurology*, *502*(1), 86–112. https://doi.org/10.1002/cne.21300

Safari, S., Ahmadi, N., Mohammadkhani, R., Ghahremani, R., Khajvand-Abedeni, M., Shahidi, S., Komaki, A., Salehi, I., & Karimi, S. A. (2021). Sex differences in spatial learning and memory and hippocampal long-term potentiation at perforant pathway-dentate gyrus (PP-DG) synapses in Wistar rats. *Behavioral and Brain Functions*, *17*(1), 9. https://doi.org/10.1186/s12993-021-00184-y

Salimpoor, V. N., Van Den Bosch, I., Kovacevic, N., McIntosh, A. R., Dagher, A., & Zatorre, R. J. (2013). Interactions Between the Nucleus Accumbens and Auditory Cortices Predict Music Reward Value. *Science*, *340*(6129), 216–219. https://doi.org/10.1126/science.1231059

Savage, L. (2004). The effects of hippocampal lesions on learning, memory, and reward expectancies. *Neurobiology of Learning and Memory*, *82*(2), 109–119. https://doi.org/10.1016/j.nlm.2004.05.002

Schuman, E. M., & Madison, D. V. (1994a). Locally distributed synaptic potentiation in the hippocampus. *Science (New York, N.Y.)*, *263*(5146), 532–536. https://doi.org/10.1126/science.8290963

Schuman, E. M., & Madison, D. V. (1994b). Locally distributed synaptic potentiation in the hippocampus. *Science (New York, N.Y.)*, *263*(5146), 532–536. https://doi.org/10.1126/science.8290963

Scofield, M. D., Heinsbroek, J. A., Gipson, C. D., Kupchik, Y. M., Spencer, S., Smith, A. C. W., Roberts-Wolfe, D., & Kalivas, P. W. (2016). The Nucleus Accumbens: Mechanisms of Addiction across Drug Classes Reflect the Importance of Glutamate Homeostasis. *Pharmacological Reviews*, *68*(3), 816–871. https://doi.org/10.1124/pr.116.012484

Sjulson, L., Peyrache, A., Cumpelik, A., Cassataro, D., & Buzsáki, G. (2018). Cocaine Place Conditioning Strengthens Location-Specific Hippocampal Coupling to the Nucleus Accumbens. *Neuron*, *98*(5), 926-934.e5. https://doi.org/10.1016/j.neuron.2018.04.015

Soares-Cunha, C., de Vasconcelos, N. A. P., Coimbra, B., Domingues, A. V., Silva, J. M., Loureiro-Campos, E., Gaspar, R., Sotiropoulos, I., Sousa, N., & Rodrigues, A. J. (2020). Nucleus accumbens medium spiny neurons subtypes signal both reward and aversion. *Molecular Psychiatry*, *25*(12), 3241–3255. https://doi.org/10.1038/s41380-019-0484-3

Sosa, M., Joo, H. R., & Frank, L. M. (2020). Dorsal and Ventral Hippocampal Sharp-Wave Ripples Activate Distinct Nucleus Accumbens Networks. *Neuron*, *105*(4), 725-741.e8. https://doi.org/10.1016/j.neuron.2019.11.022

Squire, L. R. (1992). Memory and the hippocampus: A synthesis from findings with rats, monkeys, and humans. *Psychological Review*, *99*(2), 195–231. https://doi.org/10.1037/0033-295X.99.2.195

Stern, E. A., Jaeger, D., & Wilson, C. J. (1998). Membrane potential synchrony of simultaneously recorded striatal spiny neuronsin vivo. *Nature*, *394*(6692), 475–478. https://doi.org/10.1038/28848

Strange, B. A., Witter, M. P., Lein, E. S., & Moser, E. I. (2014). Functional organization of the hippocampal longitudinal axis. *Nature Reviews Neuroscience*, *15*(10), 655–669. https://doi.org/10.1038/nrn3785

Swanson, L. W., & Cowan, W. M. (1977). An autoradiographic study of the organization of the efferet connections of the hippocampal formation in the rat. *Journal of Comparative Neurology*, *172*(1), 49–84. https://doi.org/10.1002/cne.901720104

Tao, S., Wang, Y., Peng, J., Zhao, Y., He, X., Yu, X., Liu, Q., Jin, S., & Xu, F. (2021). Whole-Brain Mapping the Direct Inputs of Dorsal and Ventral CA1 Projection Neurons. *Frontiers in Neural Circuits*, *15*, 643230. https://doi.org/10.3389/fncir.2021.643230

Terranova, J. I., Yokose, J., Osanai, H., Marks, W. D., Yamamoto, J., Ogawa, S. K., & Kitamura, T. (2022). Hippocampal-amygdala memory circuits govern experience-dependent observational fear. *Neuron*, *110*(8), 1416-1431.e13. https://doi.org/10.1016/j.neuron.2022.01.019

Trouche, S., Koren, V., Doig, N. M., Ellender, T. J., El-Gaby, M., Lopes-dos-Santos, V., Reeve, H. M., Perestenko, P. V., Garas, F. N., Magill, P. J., Sharott, A., & Dupret, D. (2019). A Hippocampus-Accumbens Tripartite Neuronal Motif Guides Appetitive Memory in Space. *Cell*, *176*(6), 1393-1406.e16. https://doi.org/10.1016/j.cell.2018.12.037

Williams, E. S., Manning, C. E., Eagle, A. L., Swift-Gallant, A., Duque-Wilckens, N., Chinnusamy, S., Moeser, A., Jordan, C., Leinninger, G., & Robison, A. J. (2020). Androgen-Dependent Excitability of Mouse Ventral Hippocampal Afferents to Nucleus Accumbens Underlies Sex-Specific Susceptibility to Stress. *Biological Psychiatry*, *87*(6), 492–501. https://doi.org/10.1016/j.biopsych.2019.08.006

Wolf, M. E., & Tseng, K. Y. (2012). Calcium-permeable AMPA receptors in the VTA and nucleus accumbens after cocaine exposure: When, how, and why? *Frontiers in Molecular Neuroscience*, *5*. https://doi.org/10.3389/fnmol.2012.00072

Xia, S., Yu, J., Huang, X., Sesack, S. R., Huang, Y. H., Schlüter, O. M., Cao, J.-L., & Dong, Y. (2020). Cortical and Thalamic Interaction with Amygdala-to-Accumbens Synapses. *The Journal of Neuroscience*, *40*(37), 7119–7132. https://doi.org/10.1523/JNEUROSCI.1121-20.2020

Yang, A. K., Mendoza, J. A., Lafferty, C. K., Lacroix, F., & Britt, J. P. (2020). Hippocampal Input to the Nucleus Accumbens Shell Enhances Food Palatability. *Biological Psychiatry*, *87*(7), 597–608. https://doi.org/10.1016/j.biopsych.2019.09.007

Yang, F.-C., & Liang, K. C. (2014). Interactions of the dorsal hippocampus, medial prefrontal cortex and nucleus accumbens in formation of fear memory: Difference in inhibitory

avoidance learning and contextual fear conditioning. *Neurobiology of Learning and Memory*, *112*, 186–194. https://doi.org/10.1016/j.nlm.2013.07.017

Yu, J., Sesack, S. R., Huang, Y., Schlüter, O. M., Grace, A. A., & Dong, Y. (2022). Contingent Amygdala Inputs Trigger Heterosynaptic LTP at Hippocampus-To-Accumbens Synapses. *The Journal of Neuroscience*, *42*(34), 6581–6592. https://doi.org/10.1523/JNEUROSCI.0838-22.2022

Yuste, R. (2011). Dendritic Spines and Distributed Circuits. *Neuron*, *71*(5), 772–781. https://doi.org/10.1016/j.neuron.2011.07.024

Zhang, L., Bose, P., & Warren, R. A. (2014). Dopamine Preferentially Inhibits NMDA Receptor-Mediated EPSCs by Acting on Presynaptic D1 Receptors in Nucleus Accumbens during Postnatal Development. *PLoS ONE*, *9*(5), e86970. https://doi.org/10.1371/journal.pone.0086970

Zhou, Y., Zhu, H., Liu, Z., Chen, X., Su, X., Ma, C., Tian, Z., Huang, B., Yan, E., Liu, X., & Ma, L. (2019). A ventral CA1 to nucleus accumbens core engram circuit mediates conditioned place preference for cocaine. *Nature Neuroscience*, *22*(12), 1986–1999. https://doi.org/10.1038/s41593-019-0524-y

Zingg, B., Chou, X., Zhang, Z., Mesik, L., Liang, F., Tao, H. W., & Zhang, L. I. (2017). AAV-Mediated Anterograde Transsynaptic Tagging: Mapping Corticocollicular Input-Defined Neural Pathways for Defense Behaviors. *Neuron*, *93*(1), 33–47. https://doi.org/10.1016/j.neuron.2016.11.045

832 **FIGURES**

833 **Figure 1. Overlapping dHipp and vHipp axon terminal fields in the NAc.** a) Viral injection
834 strategy and experimental timeline. b) Injection sites in the hippocampus. Scale bar = 500µm.
835 Atlas image from (Paxinos & Franklin, 2019) c) Overlap of dHipp and vHipp axon terminal fields
836 in the NAc. Scale bar = 500µm. Atlas image from (Paxinos & Franklin, 2019) d) Close-up image
837 of overlapping dHipp and vHipp axon terminal fields within the NAc ventromedial shell (top). Scale
838 bar = 20µm. With 3-dimensional reconstruction of overlapping axon terminals (bottom). Scale bar
839 = 0.5µm

840

841 **Figure 2. dHipp^{+}/vHipp^{+}-innervated neurons in the medial NAc shell.** a) Viral targeting
842 strategy to selectively label dually innervated neurons b) Cartoon representation of singly vs
843 dually innervated neurons. c) Image of medial NAcSh depicting GCaMP-expressing cells. Scale
844 bar = 100µm. Atlas image from (Paxinos & Franklin, 2019) d) Close-up image of GCaMP-
845 expressing cells in the medial NAcSh, where neuron morphology is consistent with medium spiny
846 neurons. Scale bar = 100µm. e) Viral targeting strategy and experimental timeline to label cells
847 innervated by dHipp and vHipp. f) Cartoon representation of singly vs dually innervated neurons.
848 g) Image of cells innervated by dHipp (green) and vHipp (magenta). Dually innervated neurons
849 express both reporters and appear white. Arrowheads point out examples of dually innervated
850 neurons. Scale bar = 100µm h) Quantification of cells innervated single and dually innervated
851 neurons in the medial NAcSh across 4 slices.

852

853 **Figure 3. Individual NAc neurons are functionally innervated by dHipp and vHipp.** a) Viral
854 targeting and optogenetic approach. Electrophysiological recording strategy and representative
855 traces from a dually innervated NAc MSN. b) Similar AMPA:NMDA receptor ratios between dHipp-
856 and vHipp-MSN synapses (n=8 cells/4 mice, p=0.1953, Wilcoxon test). Scale bars on
857 representative traces = 40pA/10ms. c) PPRs recorded from dHipp-MSN and vHipp-MSN

858 synapses on dually innervated neurons (n=16 cells/10 mice, *p=0.0394, Paired t-test). Scale bars
859 on representative traces = 20pA/20ms. d) Rectification curve reveals linear relationship, indicating
860 a lack of calcium-permeable AMPA receptors (n=8 cells/4 mice). e) Rise time was calculated for
861 dHipp- and vHipp-evoked EPSCs, showcasing similar rise times (n=31 cells/12 mice, *p*=0.2877,
862 Wilcoxon test).
863
864 **Figure 4. Spatial proximity of dHipp and vHipp puncta along distal dendrites of MSN**. a)
865 Cartoon depicting optogenetic, electrophysiology, and cell-filling strategy. b) Combined and
866 separated images depicting an MSN filled with CF633 confirmed to have functional dHipp and
867 vHipp synapses, dHipp puncta (green), vHipp puncta (red). Scale bar = 5μm. c) Three-
868 dimensional reconstruction of an MSN dendritic segment (cyan) with overlapping/merged dHipp
869 (red) and vHipp (green) afferents. Scale bar = 1μm. d) Summary data showing the proportions of
870 nearest neighbor distances in a stacked bar graph. e) Nearest neighbor distances shown in 2μm
871 bins (n=9 cells/6 mice). The observed distribution differed significantly from a uniform distribution
872 (p<0.0001; Chi-square goodness-of-fit test). Dotted line indicates expected values from uniform
873 distribution.
874
875 **Figure 5. Heterosynaptic potentiation of dHipp-MSN and vHipp-MSN synapses.** a) Viral
876 expression, optogenetic, and electrophysiology strategy. b) Recording from dually innervated
877 MSNs, sequential and synchronous stimulation assay reveals non-linear summation of responses
878 (n=16 cells/10 mice, ***p*=0.0027, Wilcoxon test). Scale bars on representative traces =
879 20pA/10ms. c) Sequential and synchronous stimulation assay performed in singly innervated
880 MSNs reveals similar responses to a single wavelength of light or both wavelengths of light (n=16
881 cells/10 mice, *p*=0.4037, Wilcoxon test). Scale bars on representative traces = 20pA/10ms. d)
882 Raster plot showing failures and successes from minimal stimulation assay. Time period 300-
883 420s is synchronized light pulses. Representative traces from Cell 9 are shown above the plot.

884 Scale bars on representative traces = 30pA/20ms. e) Theoretical probability of dual success, P_{exp},
885 compared with observed dual response success, P_{obs}, during sync period (n=9 cells/5 mice,
886 *p=0.0273, Wilcoxon test).
887
888 **Figure S1. Prevention of cross-contamination when using 470nm light and the optogenetic**
889 **protein, Chrimson.** a) Mice were injected with a Chrimson-containing viral construct and slices
890 were taken at least 5 weeks after surgery to perform electrophysiology. b) A response curve was
891 generated by sampling Chrimson-evoked responses using 470nm light, showing minimal
892 responses at a laser intensity of 0.75mW, and no Chrimson-evoked response at laser intensities
893 ≤0.5mW. EPSC amplitudes were normalized to the maximum EPSC amplitude. c) Mice were
894 injected with a Chronos-containing viral construct and slices were taken at least 5 weeks after
895 surgery to perform electrophysiology. d) No responses were observed at any of the sampled light
896 intensities. Responses were also recorded in response to 470nm (1mW) to verify successful
897 targeting and stimulation (shown in green on the left).
898
899 **Figure S2. Heterosynaptic potentiation across multiple light intensities.** Recording from
900 dually innervated MSNs, sequential and synchronous stimulation assay reveals non-linear
901 summation of responses at multiple light intensities (0.5-0.7mW). (n=11 cells/3 mice, p=0.0029,
902 Friedman test with Dunn's multiple comparisons test: 0.7 vs 0.4: **p=0.0031, 0.6 vs 0.4:
903 *p=0.0300, 0.5 vs 0.4: *p=0.0494). Each line represents a cell. Black highlights a cell with no
904 change across light intensities. Red highlights a cell where potentiation score decreased with
905 increasing light intensity. Scale bars on representative traces = 20pA/20ms.

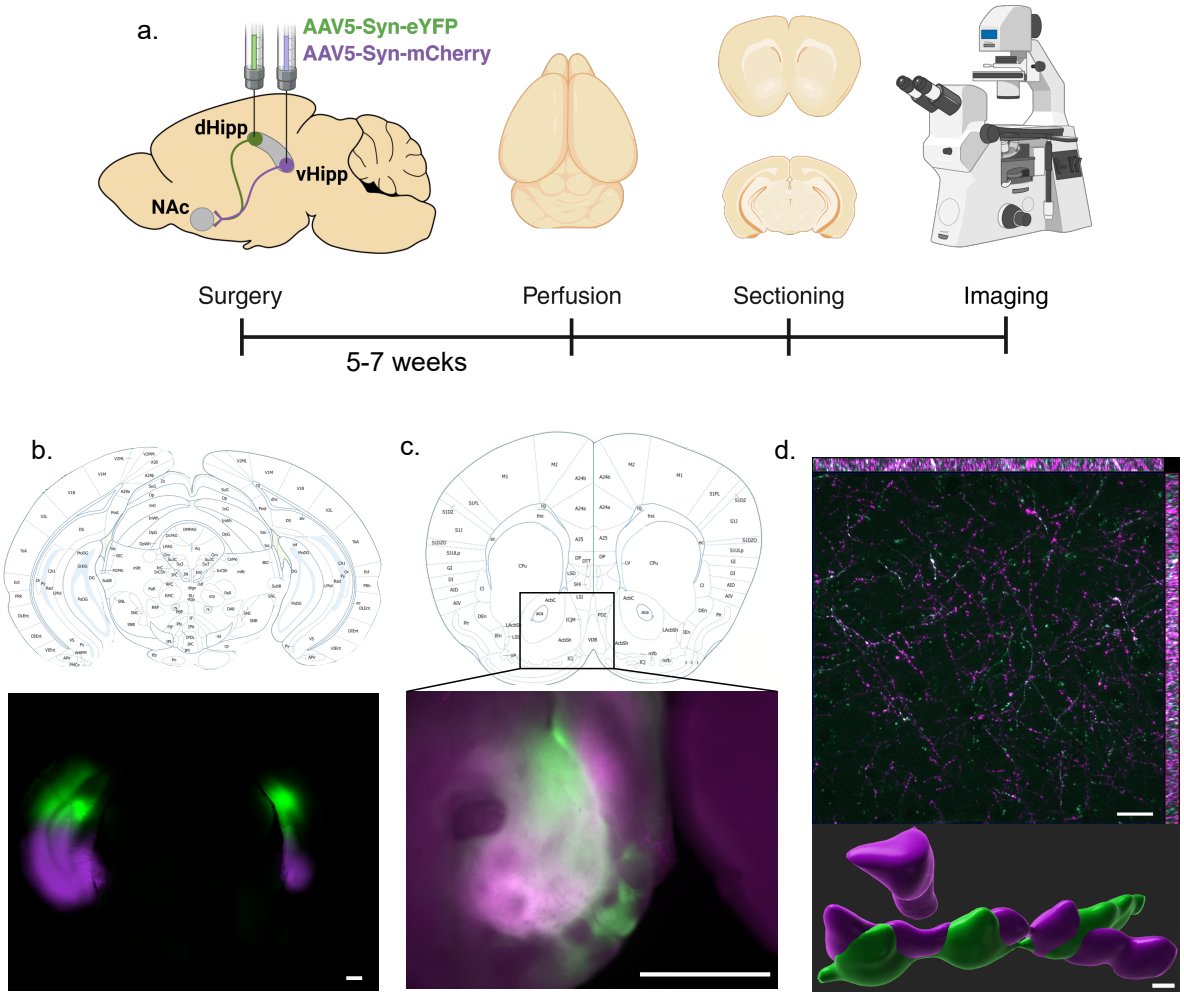
a.
AAV5-Syn-eYFP
AAV5-Syn-mCherry
dHipp
vHipp
NAc
Surgery
Perfusion
Sectioning
Imaging
5-7 weeks
b.
c.
d.

Figure 1

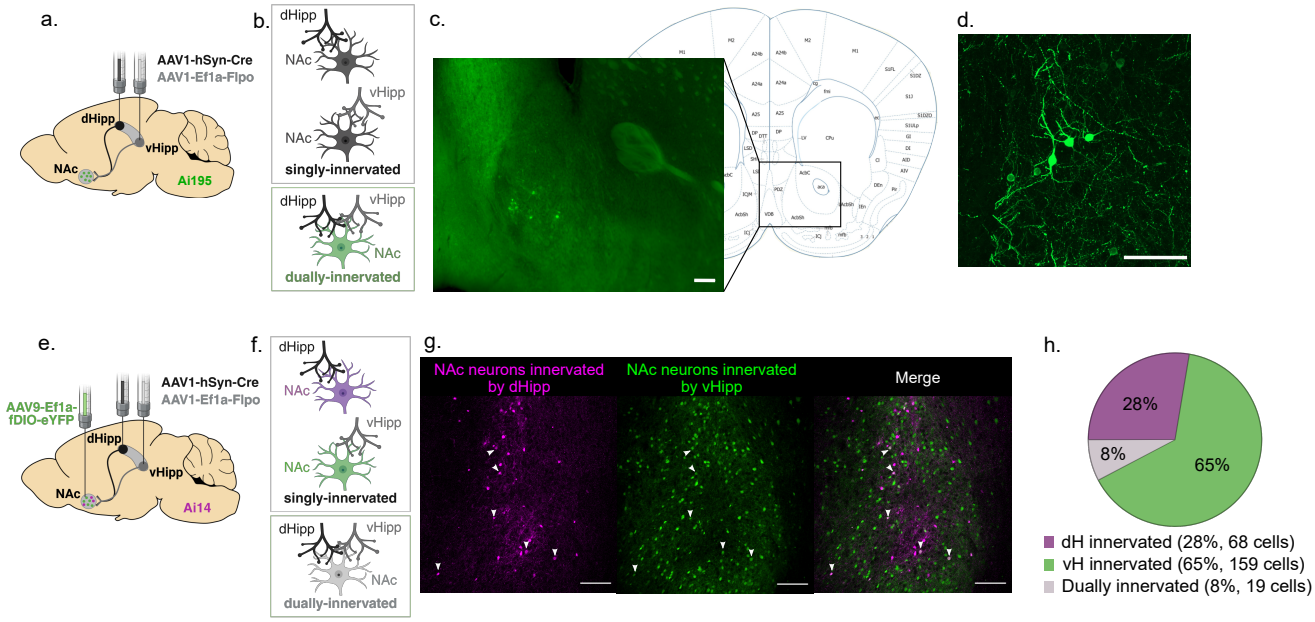
a.
AAV1-hSyn-Cre
AAV1-Ef1a-Flpo
dHipp
vHipp
NAc
Ai195
b.
dHipp
NAc
vHipp
NAc
singly-innervated
dHipp
vHipp
NAc
dually-innervated
c.
d.
e.
AAV9-Ef1a-fDIO-eYFP
AAV1-hSyn-Cre
AAV1-Ef1a-Flpo
dHipp
vHipp
NAc
Ai14
f.
dHipp
NAc
vHipp
NAc
singly-innervated
dHipp
vHipp
NAc
dually-innervated
g.
NAc neurons innervated by dHipp
NAc neurons innervated by vHipp
Merge
h.
28%
8%
65%
dH innervated (28%, 68 cells)
vH innervated (65%, 159 cells)
Dually innervated (8%, 19 cells)

Figure 2

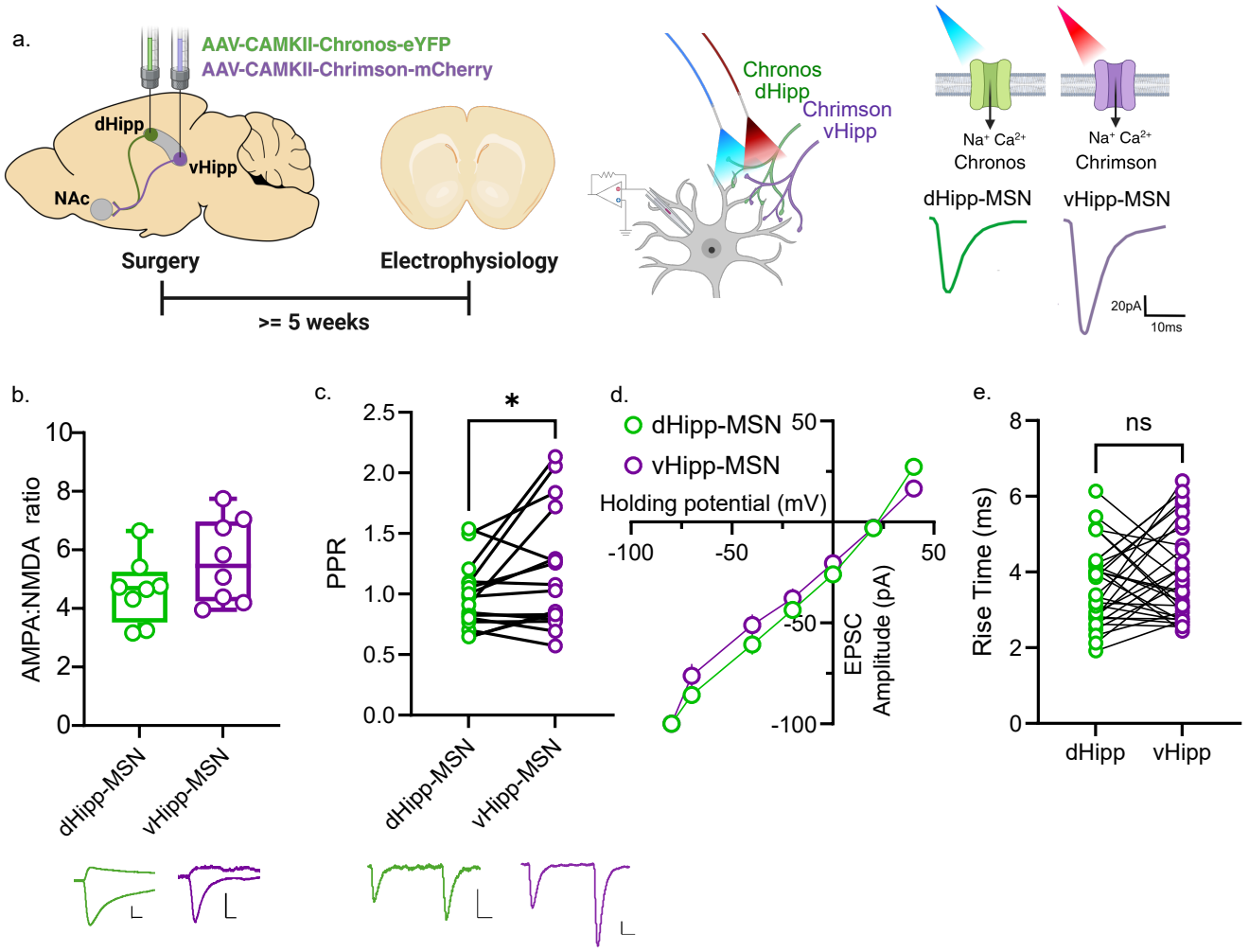
a.
AAV-CAMKII-Chronos-eYFP
AAV-CAMKII-Chrimson-mCherry
dHipp
vHipp
NAc
Surgery
Electrophysiology
>= 5 weeks
Chronos
dHipp
Chrimson
vHipp
Na+ Ca2+
Chronos
Na+ Ca2+
Chrimson
dHipp-MSN
vHipp-MSN
20pA
10ms
b.
AMPA:NMDA ratio
dHipp-MSN
vHipp-MSN
c.
PPR
*
dHipp-MSN
vHipp-MSN
d.
dHipp-MSN
vHipp-MSN
Holding potential (mV)
EPSC Amplitude (pA)
e.
Rise Time (ms)
ns
dHipp
vHipp

Figure 3

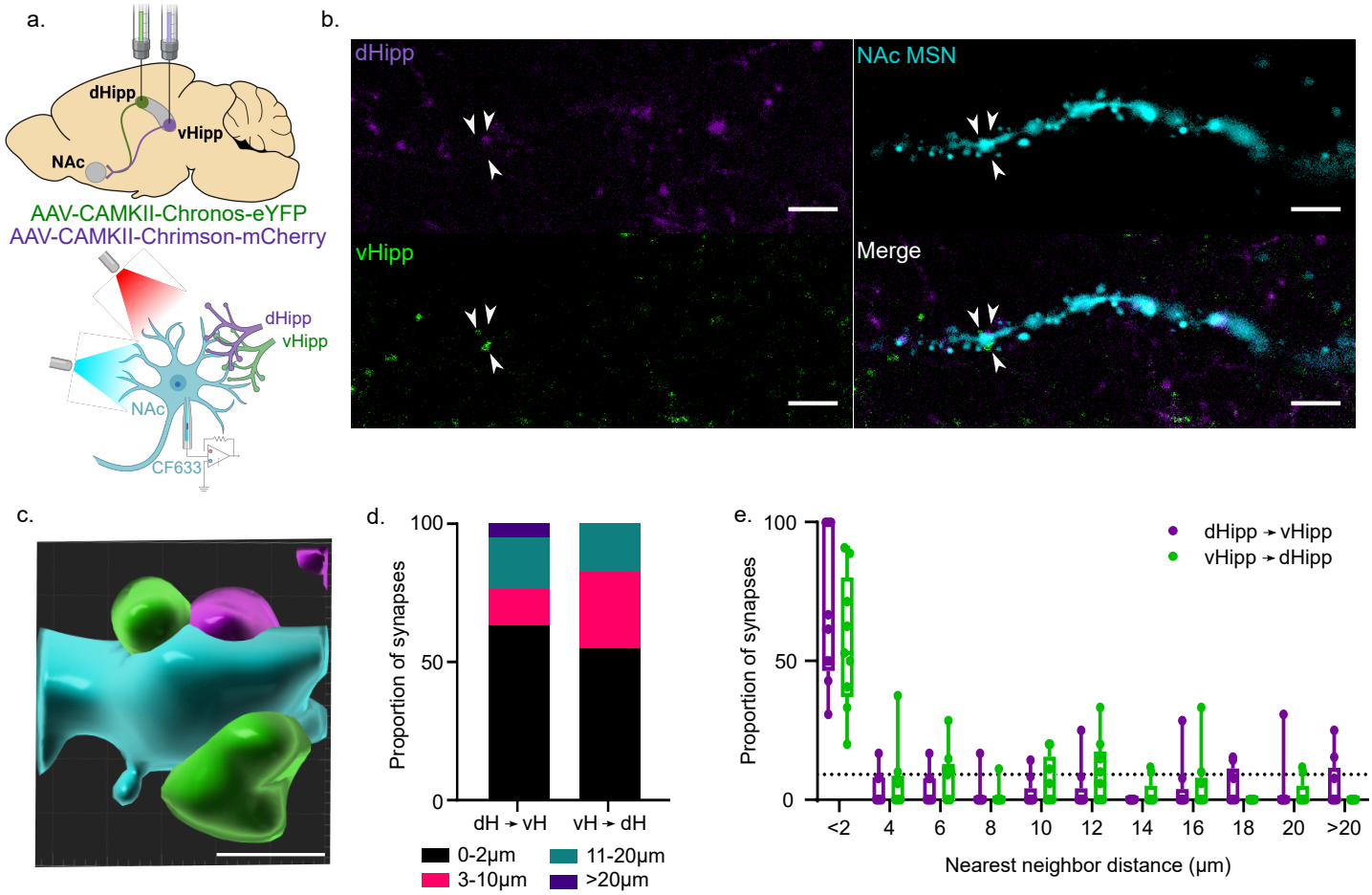
a.
dHipp
vHipp
NAc
AAV-CAMKII-Chronos-eYFP
AAV-CAMKII-Chrimson-mCherry
dHipp
vHipp
NAc
CF633
b.
dHipp
NAc MSN
vHipp
Merge
c.
d.
Proportion of synapses
100
50
0
dH → vH
vH → dH
0-2μm
3-10μm
11-20μm
>20μm
e.
Proportion of synapses
100
50
0
dHipp → vHipp
vHipp → dHipp
<2
4
6
8
10
12
14
16
18
20
>20
Nearest neighbor distance (μm)

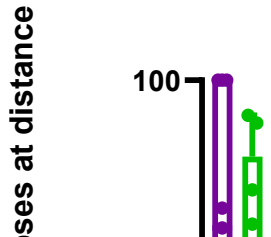
ses at distance
100

Figure 4

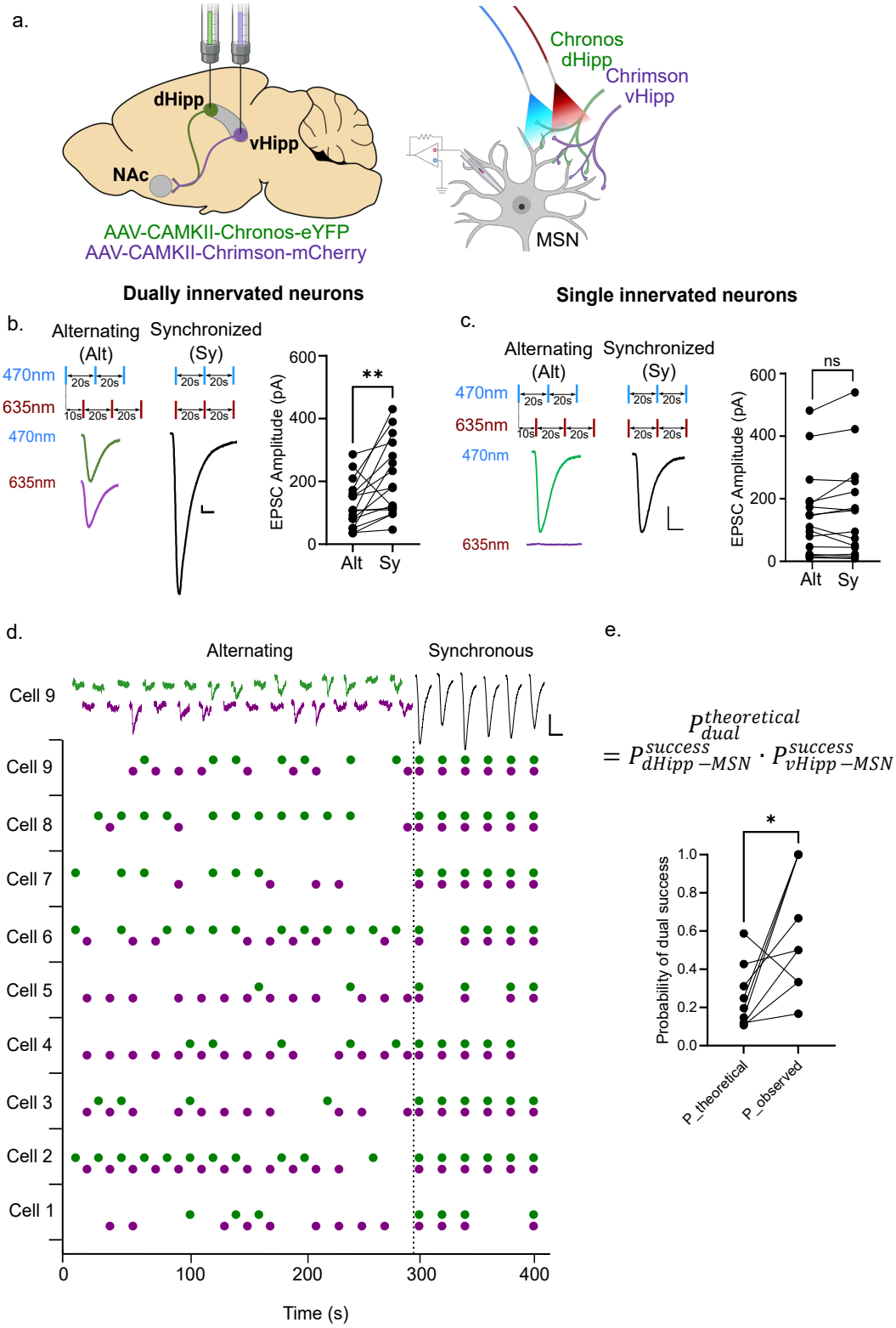
a.
dHipp
vHipp
NAc
AAV-CAMKII-Chronos-eYFP
AAV-CAMKII-Chrimson-mCherry
Chronos
dHipp
Chrimson
vHipp
MSN
Dually innervated neurons
Single innervated neurons
b.
Alternating (Alt)
Synchronized (Sy)
470nm
635nm
20s
10s
EPSC Amplitude (pA)
**
Alt
Sy
c.
ns
d.
Alternating
Synchronous
Cell 9
Cell 8
Cell 7
Cell 6
Cell 5
Cell 4
Cell 3
Cell 2
Cell 1
Time (s)
e.
$P_{dual}^{theoretical} = P_{dHipp-MSN}^{success} \cdot P_{vHipp-MSN}^{success}$
*
Probability of dual success
P_theoretical
P_observed

Figure 5

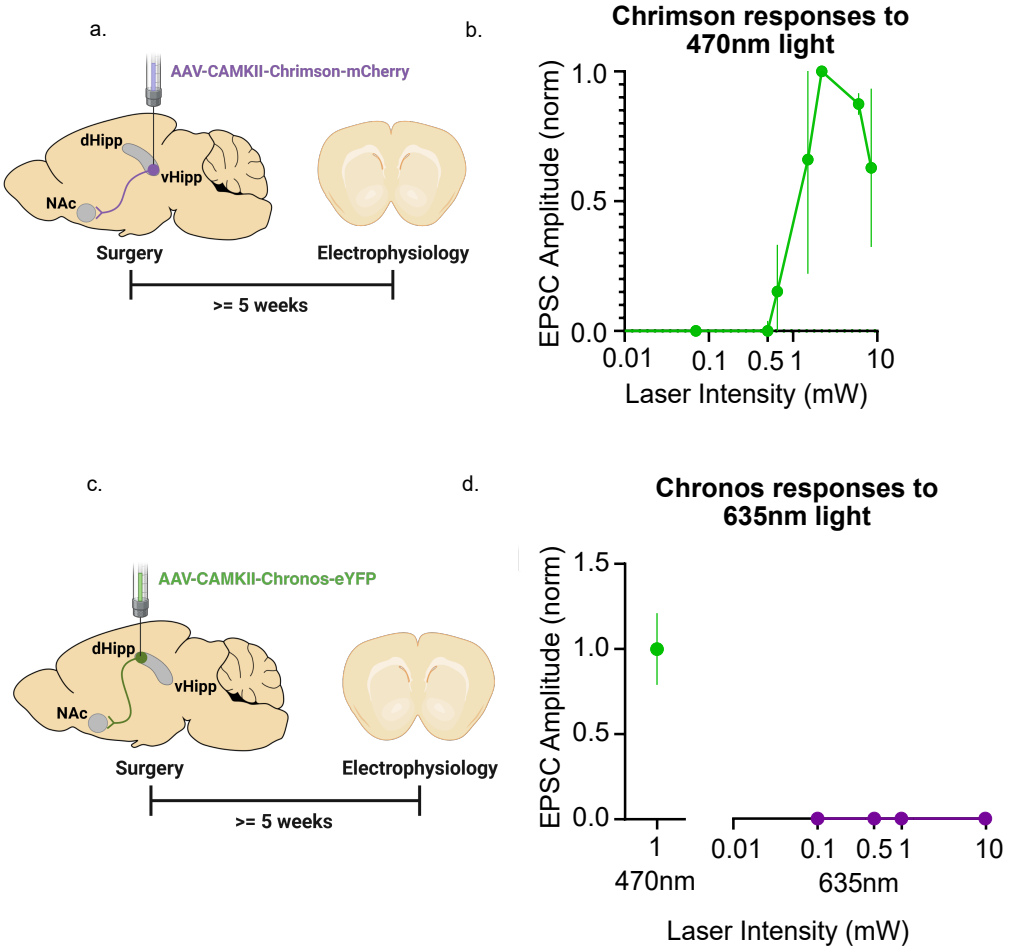

Supplemental Figure 1

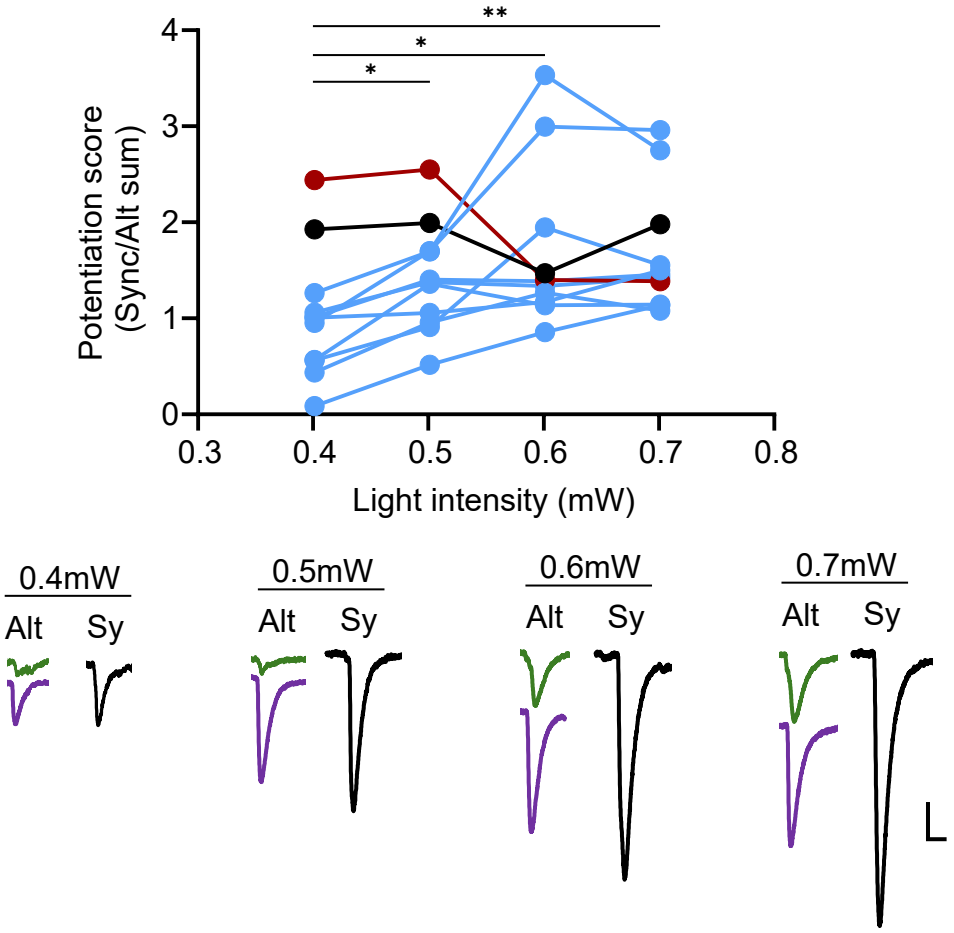

Supplemental Figure 2